The importance of NOx control for peak ozone mitigation based on a sensitivity study using CMAQ-HDDM-3D model during a typical episode over the Yangtze River delta region, China.

WANG, Y., YALUK, E.A., CHEN, H., JIANG, S., HUANG, L., ZHU, A., XIAO, S., XUE, J., LU, G., BIAN, J., KASEMSAN, M., ZHANG, K., LIU, H., TONG, H., OOI, M.C.G., CHAN, A. and LI, L.

2022

Yangjun Wang and Elly Arukulem Yaluk contributed equally to this work.

Key Points:

- The O_3 chemically produced in the zone above 40 m contributed significantly to the surface O_3 through vertical transport
- O_3 sensitivity to NO_x was high and positive in the afternoon over most of Yangtze River Delta region, including urban areas
- Controlling NO_x emissions is an important way to reduce peak O_3, and the more NO_x is reduced, the faster the decrease of peak O_3

The Importance of NOx Control for Peak Ozone Mitigation Based on a Sensitivity Study Using CMAQ-HDDM-3D Model During a Typical Episode Over the Yangtze River Delta Region, China

Yangjun Wang[1,2], Elly Arukulem Yaluk[1,2], Hui Chen[1,2], Sen Jiang[1,2], Ling Huang[1,2], Ansheng Zhu[1,2], Shilin Xiao[1,2], Jin Xue[1,2], Guibin Lu[3], Jinting Bian[1,2], Manomaiphiboon Kasemsan[4,5], Kun Zhang[1,2], Hanqing Liu[1,2], Huanhuan Tong[1,2], Maggie Chel Gee Ooi[6], Andy Chan[7], and Li Li[1,2]

[1]School of Environmental and Chemical Engineering, Shanghai University, Shanghai, China, [2]Key Laboratory of Organic Compound Pollution Control Engineering, Shanghai University, Shanghai, China, [3]School of Economics, Shanghai University, Shanghai, China, [4]The Joint Graduate School of Energy and Environment, King Mongkut's University of Technology, Bangkok, Thailand, [5]Center of Excellence on Energy Technology and Environment, Ministry of Higher Education, Science, Research and Innovation, Bangkok, Thailand, [6]Institute of Climate Change (IPI), National University of Malaysia (UKM), Selangor, Malaysia, [7]Department of Civil Engineering, University of Nottingham Malaysia, Selangor, Malaysia

Abstract In recent years, ground-level ozone (O_3) has been one of the main pollutants hindering air quality compliance in China's large city-clusters including the Yangtze River Delta (YRD) region. In this work, we utilized the process analysis (PA) and the higher-order decoupled direct method (HDDM-3D) tools embedded in the Community Multiscale Air Quality model (CMAQ) to characterize O_3 formation and sensitivities to precursors during a typical O_3 pollution episode over the YRD region in July 2018. Results indicate that gas-phase chemistry contributed dominantly to the ground-level O_3 although a significant proportion was chemically produced at the middle and upper boundary layer before reaching the surface via diffusion process. Further analysis of the chemical pathways of O_3 and O_x formation provided deep insights into the sensitivities of O_3 to its precursors that were consistent with the HDDM results. The first-order sensitivities of O_3 to anthropogenic volatile organic compounds (AVOC) were mainly positive but small, and temporal variations were negligible compared with those to NO_x. During the peak O_3 time in the afternoon, the first- and second-order sensitivities of O_3 to NO_x were significantly positive and negative, respectively, suggesting a convex response of O_3 to NO_x over most areas including Shanghai, Hangzhou, Nanjing and Hefei. These findings further highlighted an accelerated decrease in ground-level O_3 in the afternoon corresponding to continuous decrease of NO_x emissions in the afternoon. Therefore, over the YRD region including its metropolises, NO_x emission reductions will be more important in reducing the afternoon peak O_3 concentration compared with the effect of VOC emission control alone.

Plain Language Summary Ground-level ozone (O_3) is formed primarily from photochemical reactions between volatile organic compounds (VOCs) and nitrogen oxides (NO_x). Besides, O_3 and other pollutants also frequently undergo various other processes such as vertical/horizontal transport and deposition. These chemical and physical processes cause the complexity of O_3 formation and pose challenges to its mitigation. For instance, in the Yangtze River Delta (YRD) region of eastern China, ground-level O_3 has been among the main pollutants hindering air quality compliance. In this study, advanced modeling techniques based on the state-of-science community multiscale air quality model were utilized to understand at a regional scale the nonlinear response of O_3 to NO_x and VOCs, as well as to explore the contributions of these processes to O_3 during the pollution episode between 24th and 31th July 2018 over this region. The results emphasized that O_3 sensitivity to NO_x was high and positive in the afternoon over most areas including the urban cores. This strongly indicates that NO_x emission reductions could be an important way to reduce peak O_3 and the more the reduction of NO_x, the faster the decrease of peak O_3. These findings provide important insights into the formulation of policies and regulations to mitigate O_3 pollution.

Investigation: Yangjun Wang, Elly Arukulem Yaluk
Methodology: Yangjun Wang, Elly Arukulem Yaluk, Guibin Lu, Manomaiphiboon Kasemsan
Project Administration: Li Li
Software: Yangjun Wang, Elly Arukulem Yaluk, Ling Huang, Ansheng Zhu
Supervision: Yangjun Wang
Validation: Yangjun Wang, Elly Arukulem Yaluk, Hui Chen, Sen Jiang, Shilin Xiao, Hanqing Liu
Visualization: Elly Arukulem Yaluk, Shilin Xiao, Jin Xue, Jinting Bian, Huanhuan Tong
Writing – original draft: Yangjun Wang, Elly Arukulem Yaluk
Writing – review & editing: Kun Zhang, Maggie Chel Gee Ooi, Andy Chan

1. Introduction

Ground-level ozone (O_3) is among the key pollutants linked to adverse impacts on human health (Chen et al., 2017), crop production (Pleijel et al., 2018; Y. L. Wang et al., 2022) and climate change (Watson et al., 1990). In recent years, increased attention from the scientific and regulatory communities have been drawn by the elevated values of O_3 concentrations that frequently violated the National Ambient Air Quality Standards (NAAQS) in many Chinese cities, especially in eastern China (Shu et al., 2020; M. Wang et al., 2020; Xu et al., 2021). With the recent yearly reduction of $PM_{2.5}$ concentrations, O_3 compliance has been the main goal of China's atmospheric environmental management.

A number of studies have revealed the important role of meteorological processes in the formation of high O_3 concentration. J. Zhang et al. (2021) indicated that the stratospheric intrusions that frequently occur during spring, effectively transported cold air masses with high ozone from the lower stratosphere downwards into the upper troposphere over the North China Plain (NCP). In Hong Kong, it was previously reported that O_3 transported from southeastern or southern China affected the region when high-pressure system and tropical cyclone prevailed (Lin et al., 2021). Moreover, the O_3 variation during 2015–2017 in eastern China was mainly associated with the north-south movement of the subtropical high (H. Liu et al., 2021). Zhan et al. (2020) further demonstrated that landfall typhoons can significantly affect summertime O_3 in the Yangtze River Delta (YRD) region, because the O_3-rich air transported from the lower stratosphere coupled with strong photochemical reactions after the passing of a typhoon, which leads to high concentration of O_3 in the lower troposphere. Still in another study, Hu et al. (2018) illustrated that the vertical mixing in the convective boundary layer uniformly redistributed O_3 downwards from the upper levels via the entrainment of O_3-rich air in the residual layer to the O_3-poor air at the ground, which explained a severe O_3 pollution episode that occurred during the summer of 2017 in the western part of YRD region.

Aside from the impact of meteorological processes, the emissions of nitrogen oxides ($NO_x = NO_2 + NO$) and volatile organic compounds (VOCs) are closely related to the formation of O_3 pollution events (Brancher, 2021; Y. Liu et al., 2020). O_3 as an indicator pollutant of photochemical smog, is produced via a series of chemical reactions involving NO_x and VOCs in the presence of solar radiation. Furthermore, the response of O_3 to these precursor emissions is highly complex and nonlinear (Wei et al., 2019). Nonetheless, the effectiveness of emission controls to mitigate O_3 pollution depends on the chemical sensitivity of O_3 formation as either NO_x limited or VOC limited. In the VOC-limited (or NO_x-saturated) regime, VOC emission reduction decreases the supply of organic radicals (RO_2) produced from OH-initiated degradation of VOCs to oxidize NO to NO_2, and subsequently lowering the concentration of O_3. In the NO_x-limited (or VOC-saturated) regime, a reduction in NO_x emissions weakens NO_2 photolysis (a primary source of free oxygen atoms), which leads to a reduction of O_3 that would otherwise be produced from a reaction of the free oxygen atoms with O_2 (T. Wang et al., 2017). In a nutshell, cutting down NO_x and VOCs emissions reduces ambient O_3 in the NO_x-limited and VOCs-limited regimes, respectively. Therefore, understanding the sensitivities of O_3 to these precursors is an important prerequisite for the formulation of effective emission control strategies.

Several methods including observation-based approaches and air quality models (AQMs) have been broadly used to investigate the sensitivity of O_3 to its precursors. For instance, O_3 production efficiency (OPE) and photochemical indicators involving the ratios of H_2O_2/NO_z (or H_2O_2/HNO_3), $HCHO/NO_y$, $HCHO/NO_2$ among others, are widely used to evaluate the O_3 chemical regime based on in situ (D. R. Li et al., 2021; Mao et al., 2010; Ren et al., 2013) or satellite observations (Jin & Holloway, 2015). Observation-based models (OBM), which combines in situ observations and chemical box modeling, have also been widely applied in China (Lyu et al., 2016; Pan et al., 2015; Xue et al., 2014). However, these methods are often limited in temporal and spatial extent, and exclude the impacts of physical processes such as vertical and horizontal transport. Yet, these physical processes exert significant influence on O_3 formation. These drawbacks are however addressed effectively by AQMs, for example, in the community multiscale air quality (CMAQ) model, the comprehensive air quality model with extensions (CAMx) and the Weather Research and Forecasting (WRF) model coupled with Chemistry (WRF-Chem). In fact, AQMs can reproduce the entire processes of O_3 formation across consecutive spatial and temporal scales with a chemical mechanism, emission inventory and meteorology fields as the main inputs.

Compared to the other approaches, AQM-based sensitivity analysis are currently more suited to support rigorous air quality management decisions (Cohan & Napelenok, 2011; Huang et al., 2019), especially after advanced

sensitivity analysis tools such as the (higher-order) decoupled direct method in three dimension (HDDM-3D) were instrumented into some of the AQMs (Luecken et al., 2018; Yarwood et al., 2013; W. Zhang et al., 2015). Considering the traditional AQM-based brute force method (BFM) for sensitivity analysis, HDDM has been consistently found to be more flexible in implementation, and computationally efficient in capturing nonlinearities and simulation of more sensitivity parameters (Huang et al., 2017; Shen et al., 2021; W. Zhang et al., 2012).

The YRD region, which is among the most developed and densely populated regions in eastern China, has in the recent past experienced significant deterioration of summertime O_3 pollution due to changes in NO_x and anthropogenic VOC (AVOC) emissions (Y. Liu & Wang, 2020; Xu et al., 2021; Yu et al., 2019). Within the YRD region, some studies have previously investigated the pollution mechanisms and the O_3 formation regimes in Shanghai (L. Li et al., 2011; Tan et al., 2019; Xue et al., 2014), Nanjing (Ding et al., 2013; M. Wang et al., 2020) and Hangzhou (Feng et al., 2019; Han et al., 2019). According to these studies, O_3 formation in this region has been consistently found to be VOC-limited in urban areas; NO_x-limited conditions generally dominate the rural areas; and the transition regime has been (scantly) reported in some urban and suburban locations. However, most of these studies were mainly based on OBMs, which as mentioned above have inherent limitations that can only explain O_3-NO_x-VOCs sensitivity for specific locations rather than at a regional scale. Besides, most of these studies excluded the impacts of important meteorological processes that have a significant influence on O_3 formation.

Furthermore, the inherent geographical position of YRD on the southeastern coast of China, predisposes the region to the obvious impacts of major synoptic systems in summer such as the western Pacific subtropical high (WPSH), and the frequent typhoons occasioned by the subtropical monsoon climate (Zhao et al., 2022). Severe O_3 pollution episodes over the YRD are often related to the landfall typhoons and/or the WPSH (Shu et al., 2016), and the formation of O_3 during these episodes have been investigated from the physical processes perspective rather than focusing on the sensitivities of O_3 to its precursors (Jiang et al., 2021; Zhan et al., 2020). Reducing the concentrations of O_3 during such severe and frequent pollution episodes is quite important for the government to attain the national ambient air quality standards (NAAQS). Actually, O_3-precursors sensitivities along with the physical process contributions during this kind of episodes are highly needed for governments to develop effective emission control policy targeting O_3 mitigation. Therefore, this work aims to reveal the sensitivities of O_3 to its main precursors (NO_x and VOCs) along with the process analysis (PA) during a typical O_3 pollution episode, which was impacted by landfall typhoons in the YRD region. This will fill the existing knowledge gap and eventually provide scientific insights for effective pollution control measures.

In this study, we simulate a typical O_3 pollution episode in the YRD region that occurred between 24 and 31 July 2018, during which high O_3 levels were found to be related to landfall typhoons. Based on the WRF and CMAQ models, we applied the HDDM-3D and the PA tools embedded in CMAQ to provide a detailed analysis of the O_3-VOCs-NO_x sensitivities and chemical pathways of O_3 formation for this severe O_3 episode. The contributions of physical and chemical processes in the formation of O_3 were analyzed to provide a comprehensive understanding of both spatial and temporal responsiveness of O_3 to NO_x and VOCs emissions over the YRD region. This enabled a precise identification of the O_3 sensitivity regimes, where effective science-based abatement options can be applied to mitigated against such frequent summertime O_3 pollution episodes in the YRD region, and to further speed up the process of China's air quality compliance.

2. Methodology

2.1. Model Systems and Data

In this work, CMAQv5.3.2 was used to simulate the air quality during the typical O_3 pollution episode from 24 to 31 July 2018, and HDDM-3D and process analysis (PA) tools embedded in the CMAQ model were used to examine the O_3-VOCs-NO_x sensitivities and the main contributors to O_3, respectively. We applied the Lambert Conformal map projection for three domains with horizontal resolutions of 36, 12 and 4 km, respectively, as shown in Figure 1. These domains were vertically divided into 14 layers. The innermost/target domain covers the entire YRD region. The domain setup and emission inventory used in this work are the same with what were utilized in a recent study (L. Li et al., 2020). For the regions outside YRD, we applied the Multi-resolution Emission Inventory of China model (MEIC, http://meicmodel.org/), while the natural/biogenic emissions for all the three domains were estimated by the Model of Emissions of Gases and Aerosols from Nature (MEGANv3.1, http://bai.ess.uci.edu/megan). Additionally, CMAQ-ready emission files were prepared using the Sparse Matrix
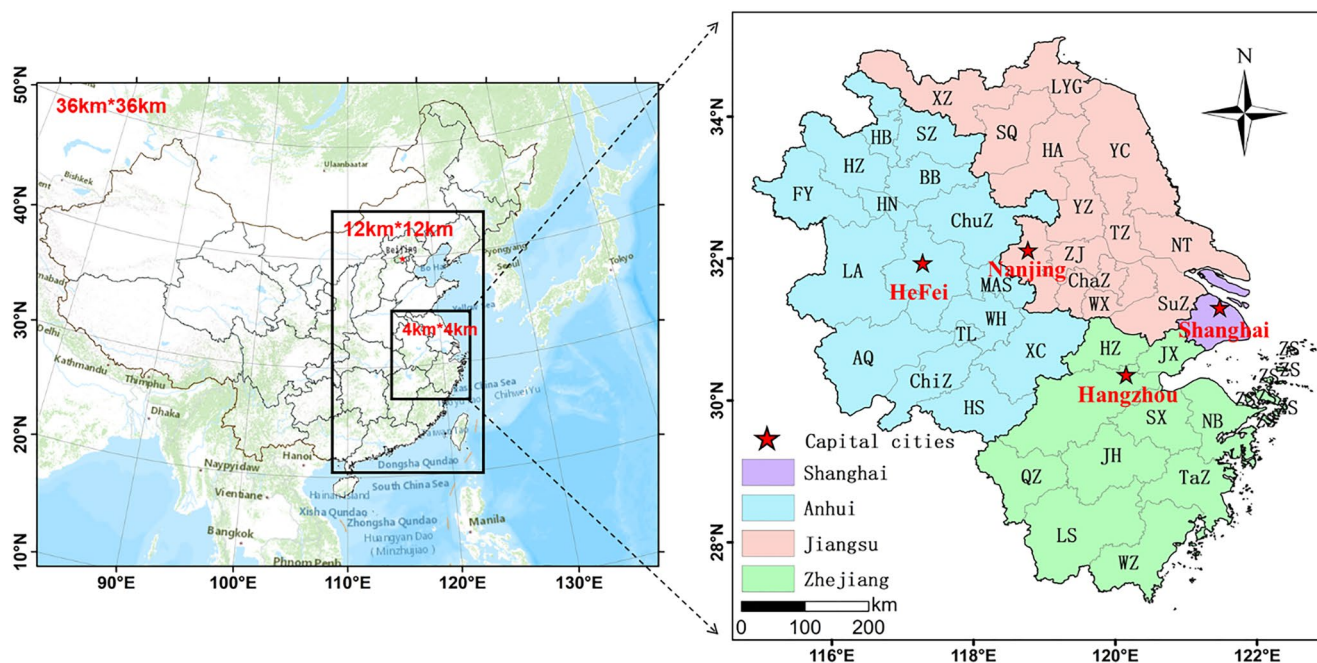
Figure 1. The domains of the model system used in this study. The 41 cities in Yangtze River Delta region are: AQ (Anqing); BB (Bengbu); BZ (Bozhou); ChaZ (Changzhou); FY (Fuyan); HZ (Huzhou); HA (Huaian); HB (Huaibei); HN (Huainan); ChiZ (Chizhou); HS (Huangshan); JX (Jiaxing); JH (Jinhua); LS (Lishui); LYG (Lianyungang); LA (Luan); NT (Nantong); NB (Ningbo); QZ (Quzhou); SX (Shaoxing); SuZ (Suzhou in Jiangsu province); TaZ (Taizhou in Zhejiang province); TZ (Taizhou in Jiangsu province); TL (Tongling); WZ (Wenzhou); WX (Wuxi); WH (Wuhu); SQ (Suqian); SZ (Suzhou in Anhui province); XZ (Xuzhou); XC (Xuancheng); YC (Yancheng); ChuZ (Chuzhou); YZ (Yangzhou); ZJ (Zhenjiang); ZS (Zhoushan); and MAS (Maanshan), Shanghai, Hangzhou, Nanjing, and Hefei are the provincial capital cities (red star).

Operator Kernel Emissions (SMOKE), and the meteorology inputs were generated by the WRF version 4.0 (https://www.mmm.ucar.edu/wrf-model-general). The weather observational data sets ds351.0 and ds461.0 used for the assimilation of WRF simulation were obtained from the research data archive maintained by the National Center for Atmospheric Research (NACR) (https://rda.ucar.edu/), while the NCEP FNL operational model global tropospheric analyses data set ds083.2 was the input data for the WRF simulation.

Model performance was evaluated based on statistical metrics including the mean bias (MB), normalized MB (NMB), normalized mean error (NME), root mean square error (RMSE), the correlation coefficient (R) and the index of agreement (IOA) (see Equations S1–S6 in Supporting Information S1). For the CMAQ model performance, we obtained hourly ground measurements of the air pollutants at all the national control monitoring stations within the YRD region (Figure 1). This data was archived at a repository of China's Ministry of Ecology and Environment (MEE) (http://datacenter.mep.gov.cn). In addition, hourly meteorological observations were obtained from the China Meteorological Administration (CMA) for these cities in YRD to aid in the evaluation of WRF model performance. Overall, the results show that the observations of both the meteorological conditions and pollutant concentrations were well captured by the WRF and CMAQ model simulations, respectively. Detailed model performance evaluation and discussions are included in Supporting Information S1. To gain a deeper understanding of the mechanism of ozone formation, we selected one urban site and one suburban site in each provincial capital city in the YRD region (Figure 1) to conduct more detailed analyses of chemical and physical processes related to ozone formation. These sites (urban; suburban) are in Shanghai (JA Jing'an; DSL, Dianshan Lake), Hangzhou (WLB, Wolong bridge; XS, Xiasha), Nanjing (CCM, Caochangmen; MGB, Maigoa bridge) and Hefei (MZS, Mingzhu square; DPR, Dongpu Reservoir).

2.2. CMAQ-HDDM-3D

Like other AQMs, CMAQ numerically conserves and describes the formation and transport of air pollutants primarily by solving the advection-diffusion-reaction equations:

$$\frac{\partial C_i}{\partial t} = -\nabla \left(u C_i \right) + \nabla \left(K \nabla C_i \right) + R_i + E_i$$

$$(i = 1, 2, ..., N)$$

$$(1)$$

where C_i is the average concentration of species i at each grid cell, while u, K and N are the wind field, turbulent diffusivity tensor and number of chemical species, respectively. R_i and E_i represent the chemical reaction rates and emission rate of species i, respectively. Similarly, the numerical structure of HDDM algorithms is analogous to that of the base-model (Equation 1) as indicated by Hakami et al. (2003) and Hakami et al. (2004). Equation 2 below shows the HDDM equation that computes the sensitivity coefficients to emission rates:

$$\frac{\partial S_{ij}^{(1)}}{\partial t} = -\nabla \left(u S_{ij}^{(1)} \right) + \nabla \left(K \nabla S_{ij}^{(1)} \right) + J_i S_j + E_i'$$

$$(2)$$

where $S_j^{(1)}$ is the vector of the first-order sensitivity coefficients for changes in emission rates, and J_i is also a vector in the ith row of a Jacobian matrix representing reaction rates and interactions of different species, whereas E_i' is the emission rate (unperturbed). The implementation of this technique is greatly simplified with guaranteed consistency and enhanced efficiency, which ensures simultaneous computation of concentrations and sensitivities within a single simulation.

In this work, the CMAQ-HDDM-3D modeling system is configured to compute the sensitivity coefficients of O_3 to NO_x and VOC emissions as follows (Equation 3 and 4):

$$S^{(1)} = E_0 \frac{\partial C}{\partial e} = E_0 \frac{\partial C}{\partial \left[(1 + \Delta \varepsilon) E_0 \right]} = \frac{\partial C}{\partial \varepsilon}$$

$$(3)$$

$$S^{(2)} = E_0 \frac{\partial}{\partial e} \left(E_0 \frac{\partial C}{\partial e} \right) = \frac{\partial^2 C}{\partial \varepsilon^2}$$

$$(4)$$

where $S^{(1)}$ and $S^{(2)}$ are the first- and second-order sensitivity coefficients, respectively. ε is a scaling variable, hence both the sensitivities and concentration have same units (Hakami et al., 2003; L. Jin et al., 2008). Therefore, if for instance $S^{(1)}$ is equal to α ppb, it implies that with a $\pm 20\%$ perturbation in NO_x (or VOC) emissions, the concentration of O_3 would change by ($\pm 0.2\alpha$) ppb. The impact of larger perturbations on emissions (or any other sensitivity parameter) can be rapidly computed using Taylor series expansions (Hakami et al., 2003):

$$C_{P\left(e = E_0 + \Delta \varepsilon \cdot E_0 \right)} \approx C_{0\left(e = E_0 \right)} + \Delta \varepsilon \cdot S^{(1)} + \frac{(\Delta \varepsilon)^2}{2} \cdot S^{(2)}$$

$$(5)$$

C_p is the pollutant concentration (in our case O_3) after a fractional perturbation ($\Delta \varepsilon$) in the emissions (e) of either NO_x or VOCs. E_0 and C_0 both represent the base-case emissions and concentrations, respectively.

2.3. Ozone Sensitivity Regimes

Apart from O_3 sensitivity to NO_x and AVOC emissions, we also simulated the sensitivities of O_3 to biogenic VOC (BVOC) emissions in order to gain a broader insight into O_3 responses to its precursors during pollution episodes in the YRD region. It is noteworthy that the determination of O_3 chemical regimes and control options is based on the sensitivities of controllable emissions only (NO_x and AVOCs emission). For that reason, we used the relationship between the first-order O_3 sensitivities to NO_x ($S_{O_3\_NO_x}^{(1)}$) and AVOCs ($S_{O_3\_AVOC}^{(1)}$) to describe O_3 control regimes in line with the definitions of Sillman and West (2009) and X. Wang et al. (2011):

1. NO_x-sensitive: refers to areas where at a given time $S_{O_3\_NO_x}^{(1)}$ is greater than 5 ppb and is also greater than $S_{O_3\_AVOC}^{(1)}$.
2. VOC-sensitive: refers to areas where at a given time $S_{O_3\_AVOC}^{(1)}$ is larger than 5 ppb and is also greater than $S_{O_3\_NO_x}^{(1)}$.
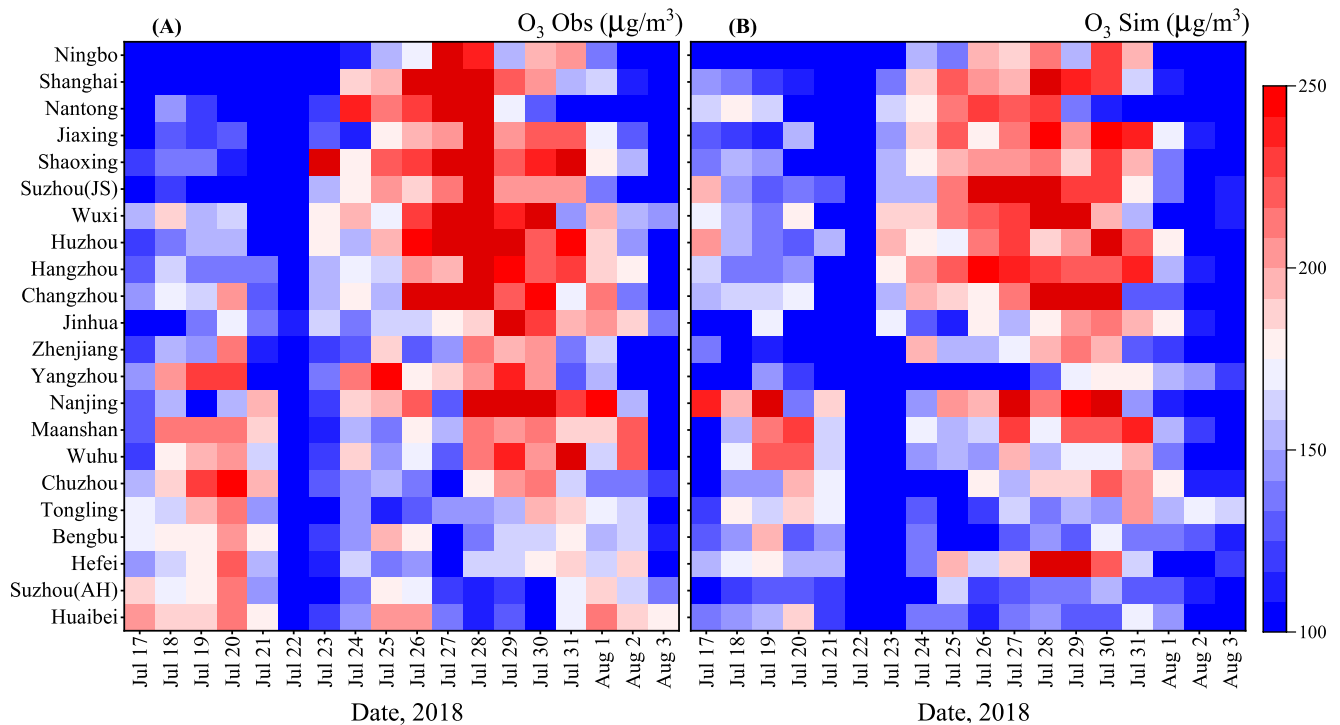
Figure 2. (a) Ground-level observations and (b) simulations of maximum hourly O_3 in selected 22 cities of Yangtze River Delta (YRD) between 17 July and 3 August 2018. The cities are ordered based on longitude (i.e., from Ningbo in the east to Huaibei in west). Suzhou (JS) is the city Suzhou in Jiangsu (JS) province and another in Anhui (AH) province with mark as Suzhou (AH). The 22 selected cities out of the 41 cities in the YRD region were obviously impacted by the typhoons. China's NAAQS for hourly maximum O_3 is 200 µg/m^3.

3. Insensitive regime: refers to the locations where at a given time both $S^{(1)}_{O_3\_NO_x}$ and $S^{(1)}_{O_3\_AVOC}$ are in the range of ±5 ppb.

4. NO$_x$-titration regime: at any given time these are locations exhibiting $S^{(1)}_{O_3\_NO_x}$ lower than −5 ppb and $S^{(1)}_{O_3\_AVOC}$ less than 5 ppb.

5. Mixed-sensitivity: this occurs in areas where at a given time both $S^{(1)}_{O_3\_AVOC}$ and $S^{(1)}_{O_3\_NO_x}$ are ≥5 ppb and both differ by less than a factor of 2.

2.4. Process Analysis

Integrated process rate (IPR) and integrated reaction rate (IRR) were computed at each model grid-cell by the PA tool to account for the hourly changes of O_3 concentrations. The IPR calculated the contributions from interactions of various atmospheric processes such as gas-phase chemistry (CHEM); dry deposition (DDEP); cloud processes with aqueous chemistry (CLDS); vertical advection (ZADV); horizontal advection (HADV); vertical diffusion (VDIF); and horizontal diffusion (HDIF). With this, we defined VERT to represent vertical transport processes (i.e., the sum of ZADV and HDIF), and HORT to represent the horizontal transport processes (i.e., the sum of HDIF and HADV). Meanwhile, IRR quantified the variation of chemical production (or loss) caused by each chemical reaction rate in the mechanism.

3. Results and Discussion

3.1. Evolution of the Ozone Pollution

Between 17 July and 1 August 2018, one pollution episode of O_3 occurred over the YRD region following a typhoon (Typhoon Ampil) that landed near Shanghai city on 22 July (Zhan et al., 2020) as shown in Figure S9b of Supporting Information S1. The variation of ground measurements and modeled daily maximum hourly O_3 concentrations during this period are shown in Figures 2a and 2b, respectively, in typical cities of YRD. It is notable that the observed concentrations of O_3 during 17−20 July in most of the cities in the
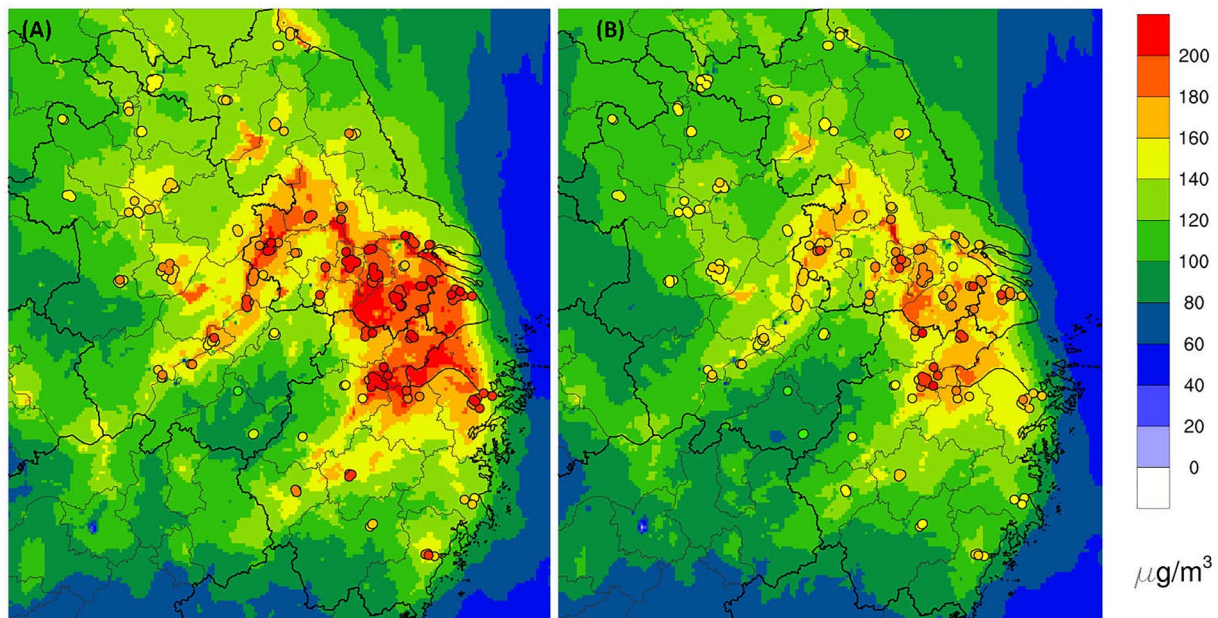
Figure 3. Observations (dots) and model simulation distributions of (a) maximum 1 hr O_3 and (b) maximum daily 8 hr average (MDA8) O_3 in the Yangtze River Delta region averaged for the episode period between 24 and 31 July 2018. The limit for China's national ambient air quality standards (NAAQS) for the 1 hr and MDA8 O_3 is 200 and 160 μg/m^3, respectively.

east of YRD (beginning from Ningbo) were relatively low (∼100 μg/m^3) as opposed to the cities in the west (Figure 2). During this period, O_3 and its precursors within the source-rich regions in the southeastern and central areas were transported into the downwind northwestern areas by the prevailing fast moving southeasterly winds. From 21 to 23 July, there was a sharp decline of O_3 in most cities, which coincided with the landing of typhoon Ampil (Zhan et al., 2020). It is well established that typhoons cause tremendous impact on the prevailing local atmospheric conditions by disrupting the chemistry, transport, deposition and related processes that are essential for the formation and accumulation of air pollutants (Shu et al., 2016). In this case, the arrival and landing of Typhoon Ampil resulted in substantial weakening of the prevailing subtropical high over the YRD region (Zhan et al., 2020). The typhoon also brought strong (fast and wild upward) winds, accompanied by heavy precipitation and low temperature, which continuously suppressed the formation of O_3, resulting in strong dispersal and removal of air pollutants and their precursors in almost the entire YRD region.

By comparison, Figures 2a and 2b show conspicuous similarity in the evolution pattern of O_3 although the simulated concentrations were slightly underestimated. Specifically, on 26 and 27, the simulated O_3 values in Shaoxing, Ningbo, and Shanghai were underestimated, whereas Yangzhou was obviously underestimated on all days. These variations could be due to sudden changes in precursor emissions or a deviation of the time-distributed profile of an emission source. For instance, the simulation of NO_2 did not capture the sudden spike of NO_2 levels observed over Shanghai on 26 and 27 July (Figure S7 in Supporting Information S1). This underestimated NO_2 corresponded with an under prediction of O_3 concentrations, which is consistent with the findings of this study with regards to controlling of NO_x emissions to reduce O_3 concentration over the YRD region as discussed in the later sections. In the other cities with better air quality, such as Chizhou and Jinhua, the simulated values are also underestimated, and this could be linked to a likely model deviation of the background concentrations.

During the severe multi-day O_3 pollution episode in the YRD region from 24 to 31 July, most cities exceeded the O_3 hourly limit of 200 μg/m^3 set by China's NAAQS (Figure 2). In fact, after the typhoon exited the YRD region, gradual onset of weak winds and slow-moving synoptic weather was experienced for several consecutive days. These occurred with drier and hotter atmospheric conditions, which facilitated the strong photochemical production and accumulation of O_3 over large areas. As a result, in addition to the maximum 1-hr O_3 exceeding the standard, the maximum daily average (MDA8) O_3 also exceeded the standard (>160 μg/m^3) over the most cities of YRD region, as shown in Figure 3. Obviously, the southeastern and central regions of the YRD,
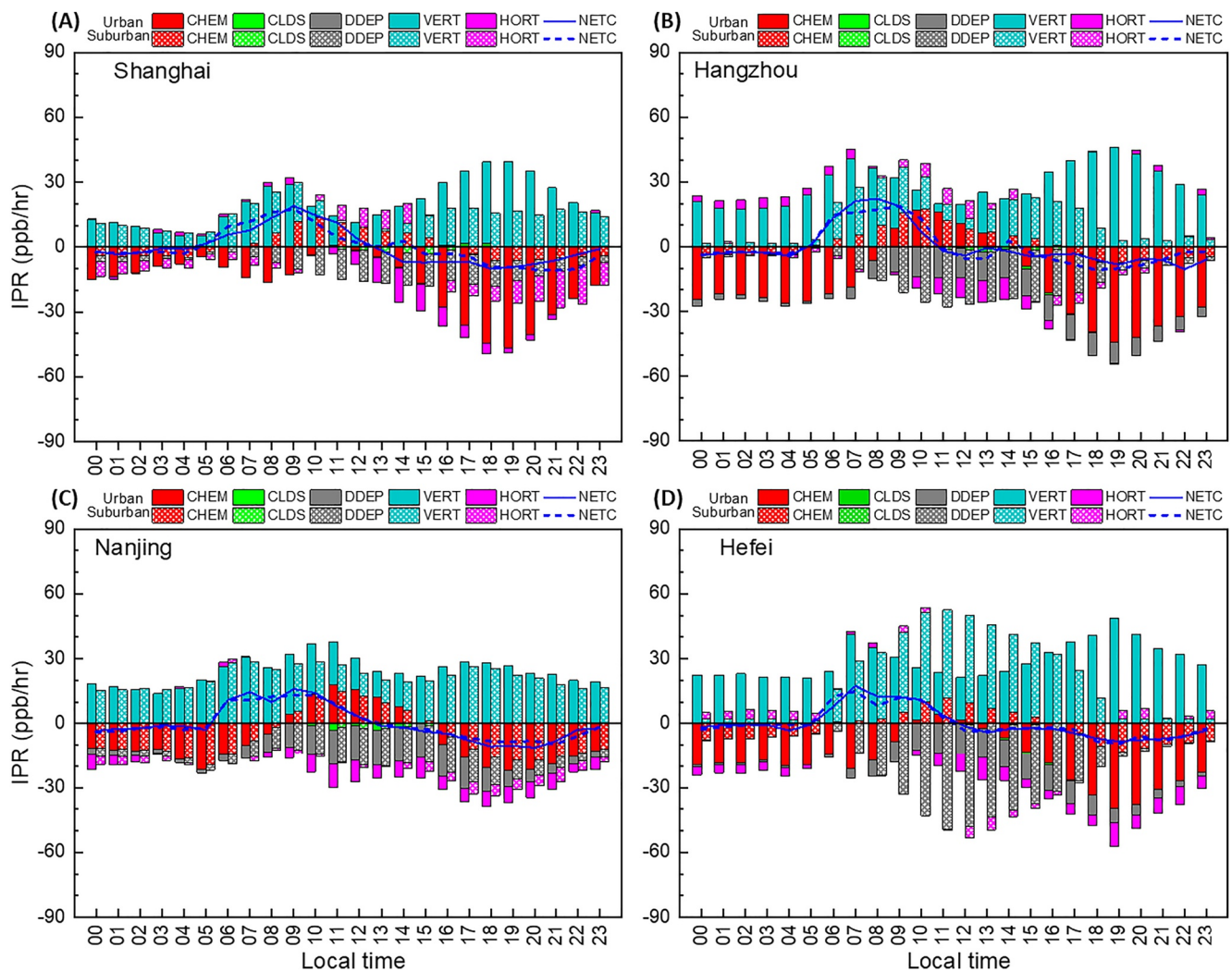
Figure 4. Diurnal variations of atmospheric process contributions to O$_3$ at the surface layer (0–40 m above ground level) averaged for the O$_3$ episode between 24 and 31 July 2018 in (a) Shanghai, (b) Hangzhou, (c) Nanjing, and (d) Hefei. The solid columns and lines indicate IPR results for typical urban sites, while the dotted columns and dashed lines are for the suburban sites. (CHEM, gas-phase chemistry; DDEP, dry deposition; CLDS, clouds and aqueous processes; ZADV, vertical advection; HADV, horizontal advection; HDIF, horizontal diffusion; VDIF, vertical diffusion; NETC, the net contribution due to all atmospheric processes).

including Hangzhou, Jiaxing, Shanghai, Shaoxing, Ningbo, and extending to Suzhou, Zhenjiang, and Nanjing, were nonattainment (Figure 3a).

All these are predominantly large urban areas, with intense human activities and strong emissions of NO$_x$ and/ or AVOCs, generally considered to constitute the core of the YRD region. Furthermore, many surrounding rural and suburban areas were nonattainment regarding to the MDA8 O$_3$ (Figure 3b), although the simulated values of MDA8 O$_3$ are slightly underestimated during this period.

3.2. Process Analysis of Ozone Formation

To illustrate the influence of the main physical and chemical processes on surface O$_3$ during the time period between 24 and 31 July 2018, we analyzed the IPR results of the first model layer (0–40 m above ground level) at the grid-cells corresponding to typical urban and suburban sites in the provincial capital cities of YRD. As shown in Figure 4, the diurnal profile of the IPR outputs in these cities present common as well as contrasting features of the main processes contributions to surface O$_3$ in the different sites.
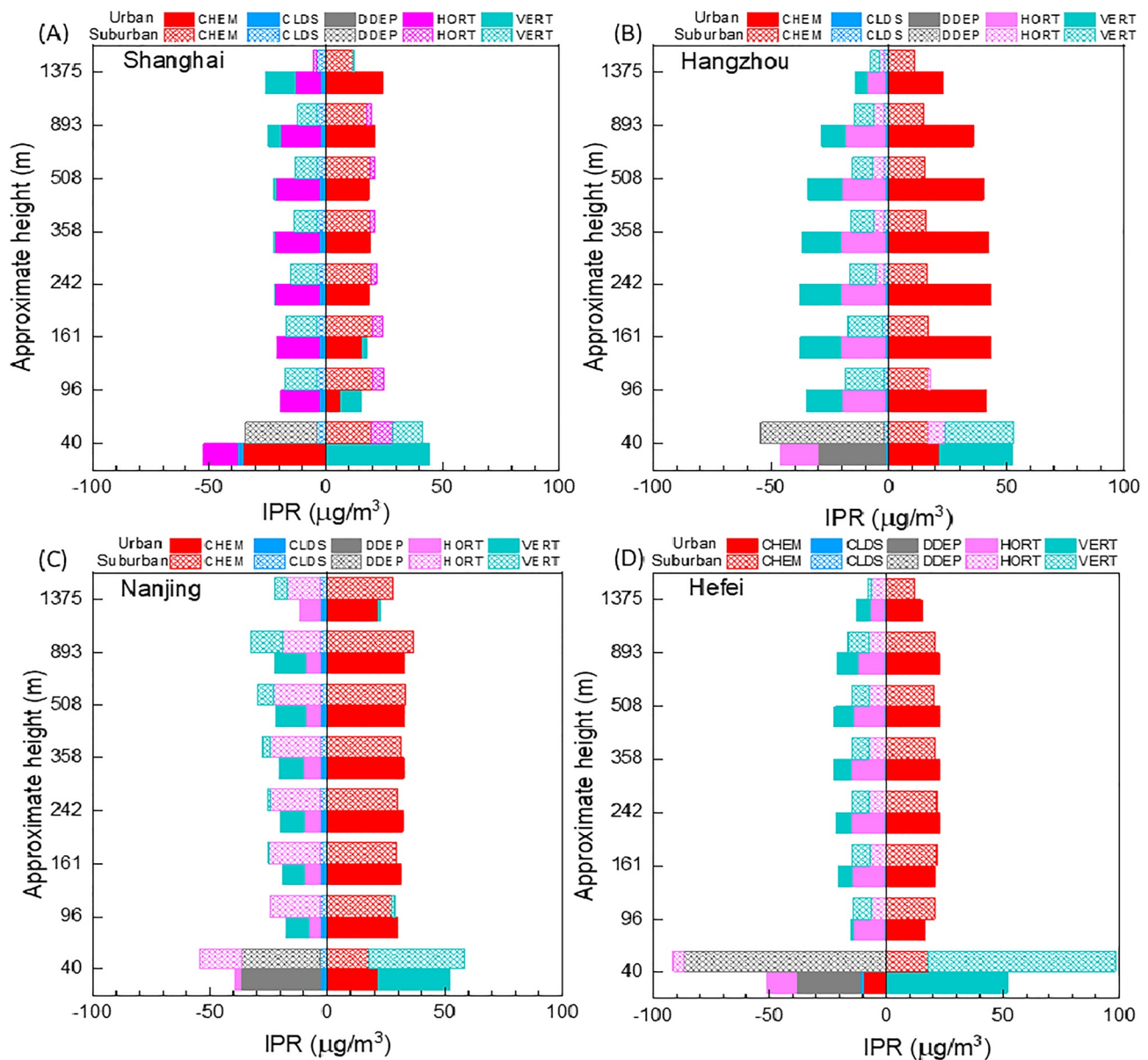
Figure 5. Changes in the contributions of main atmospheric processes during O$_3$ formation and buildup time (09:00–14:00 LT) in the bottom 8 model layers (about 0–1,375 m above ground level) for the period from 24 to 31 July 2018 in (a) Shanghai, (b) Hangzhou, (c) Nanjing, and (d) Hefei. The solid columns indicate the integrated process rate values for typical urban sites, while the dotted columns are for the suburban sites. (VERT, vertical transport; i.e., the net effect of ZADV and VDIF; HORT, horizontal transport; i.e., the net effect of HADV and HDIF; DDEP, dry deposition; CLDS, cloud processes and aqueous chemistry; and CHEM, gas-phase chemistry).

As shown in Figure 4, during the time period between 9:00 and 14:00 local time (LT), gas-phase chemistry contribution reached about 13.6, 17.4, 15.1, and 11.8 ppb/hr in typical suburban areas in Shanghai, Hangzhou, Nanjing, and Hefei, respectively. This can be linked to the increasing solar radiation and the high summer temperatures (about 30–35°C), which facilitated high photochemical formation of O$_3$. Meanwhile, in the typical urban sites, with strong NO$_x$ emissions, particularly during the traffic rush hours, CHEM contributions reached −46.6, −44.4, −21.9, and −39.6 ppb/hr in Shanghai, Hangzhou, Nanjing, and Hefei, respectively (Figure 4), suggesting the chemical destruction of O$_3$. Moreover, more O$_3$ was chemically produced in the zone with higher altitude due to the stronger radiation therein. Accordingly, the contributions of vertical transport via diffusion processes to surface O$_3$ from the zone with higher altitudes (e.g., above 40 m from surface) were significant (see Figure 5 and subsequent discussion). As shown in Figure 4, the contribution of vertical transport at the typical urban

(suburban) sites of Shanghai, Hangzhou, Nanjing, and Hefei averaged about 39.6 (19.3), 46.0 (22.1), 30.8 (28.5), and 48.9 (41.2) ppb/hr, respectively.

In general, the main features of the diurnal evolution shown in Figure 4 can be summarized as follows: (a) The net effect of the process contributions is close to zero, with vertical diffusion as the main source, and chemical destruction of O_3 as the main sink before 6:00 LT at all the urban and suburban sites of the provincial capital cities. (b) Just after sunrise (about 6:00–7:00 LT), there was a sudden increase in vertical transport contribution to O_3 for each site. Understandably, a stable and shallow boundary layer that forms near the surface at night trapped high concentrations of O_3. More specifically, with the disappearance of this residual layer after sunrise and the subsequent development of the daytime convective boundary layer, the O_3 that was trapped became redistributed from the upper "O_3-rich" zone to the ground-level "O_3-poor" zone. (c) The chemical contributions to ground-level ozone (about 40 m below in the vertical direction) is negative both at night and in the late afternoon, that is, surface O_3 is chemically depleted, not generated, during these periods. Overall, vertical transport dominated by VDIF, was the dominant contributor/main source of surface O_3 from the upper atmosphere, whereas chemical titration was the main sinks of surface O_3 both at night and in the late afternoon in all sites.

Having noted the substantial contribution of vertical transport on surface O_3 concentration, we further explored the vertical profile of the contributions of main processes within the atmospheric boundary layer (ABL), which basically corresponds to CMAQ layers 1–8 with an approximate vertical height of 0–1,375 m above the ground level as detailed in Table S5 of Supporting Information S1. Figure 5 shows the IPR outputs averaged for each model layer during the daytime between 9:00 and 14:00 (LT), which corresponds to the O_3 formation and buildup time. Interestingly, gas-phase chemistry was the dominant process contributing positively to O_3 formation within the ABL. In addition, the positive and highest chemical contribution occurred between layers 3–7 (i.e., from about 100 m to about 900 m above ground level).

Nevertheless, different cities exhibited varied patterns and magnitudes of CHEM, DDEP, VERT and HORT. For instance, at the suburban sites of Shanghai (DSL), Hangzhou (XS), and Hefei (DPR), their CHEM contributions at layers 2–7 were relatively uniform and slightly higher than their respective first layer (Figure 5). Moreover, at both the urban and suburban sites of Nanjing, and at the urban site of Hangzhou, we also noted that CHEM contribution was obviously highest in the middle part of the ABL. This suggests a stronger photochemical generation of O_3 that could have resulted from a large amount of precursors, and which was facilitated by the stronger intensity of solar radiation at that height. Meanwhile, the O_3 formed at the upper layers is then transported horizontally to downwind areas and/or vertically to the lower layers to compensate for any O_3 losses due to the titration effect or dry deposition. This can be explained by the negative (positive) VERT contribution in the upper (bottom) layers, resulting in abundant ground-level O_3 concentrations.

In the meantime, horizontal transport of O_3 in all the four key cities was generally similar in the upper layers around the middle of the ABL (negative HORT), and was more pronounced in the urban than suburban sites except at the Nanjing sites (Figure 5). Notably, Shanghai's DSL site exhibited a positive HORT contribution in the whole ABL, indicating an obviously higher O_3 concentration in its upwind areas, and hence the ozone brought in (carried away) by the horizontal airflow was more (less). For CLDS, its contribution was generally dismal and mostly negative in the entire ABL. In Shanghai for instance, because of its proximity to the sea, the city is more prone to the abundance of water vapor and relatively more cloud cover, even when the atmosphere was generally dry and less cloudy during the study period.

We further compared the CHEM contribution to O_3 with that of odd-oxygen ($O_x = O_3 + NO_2$) for a broader perspective into the role of gas-phase chemistry during the modeled episode as shown in Figure S10 of Supporting Information S1. Generally, CHEM-O_x was higher than CHEM-O_3 at the surface-layer (0–40 m above ground level) compared to the subsequent upper layers at both the urban and suburban sites of the four representative cities, although the gap between them was significantly larger over the suburban sites than the urban sites. This is largely an indication of abundant in situ production of NO_2, which correspondingly could play an important role in formation of the regional ozone pollution. To gain an in-depth understanding on the role of chemistry and dominant mechanisms responsible for the productions of both O_3 and O_x, we analyzed the IRR results to examine the contribution of individual chemical formation or loss pathway.

Figure 6 shows the simulated diurnal IRR budgets for O_3 and O_x at the typical urban (Jing'an) and suburban (DSL) sites of Shanghai averaged for the entire ABL during the O_3 episode period. For O_x, the main production
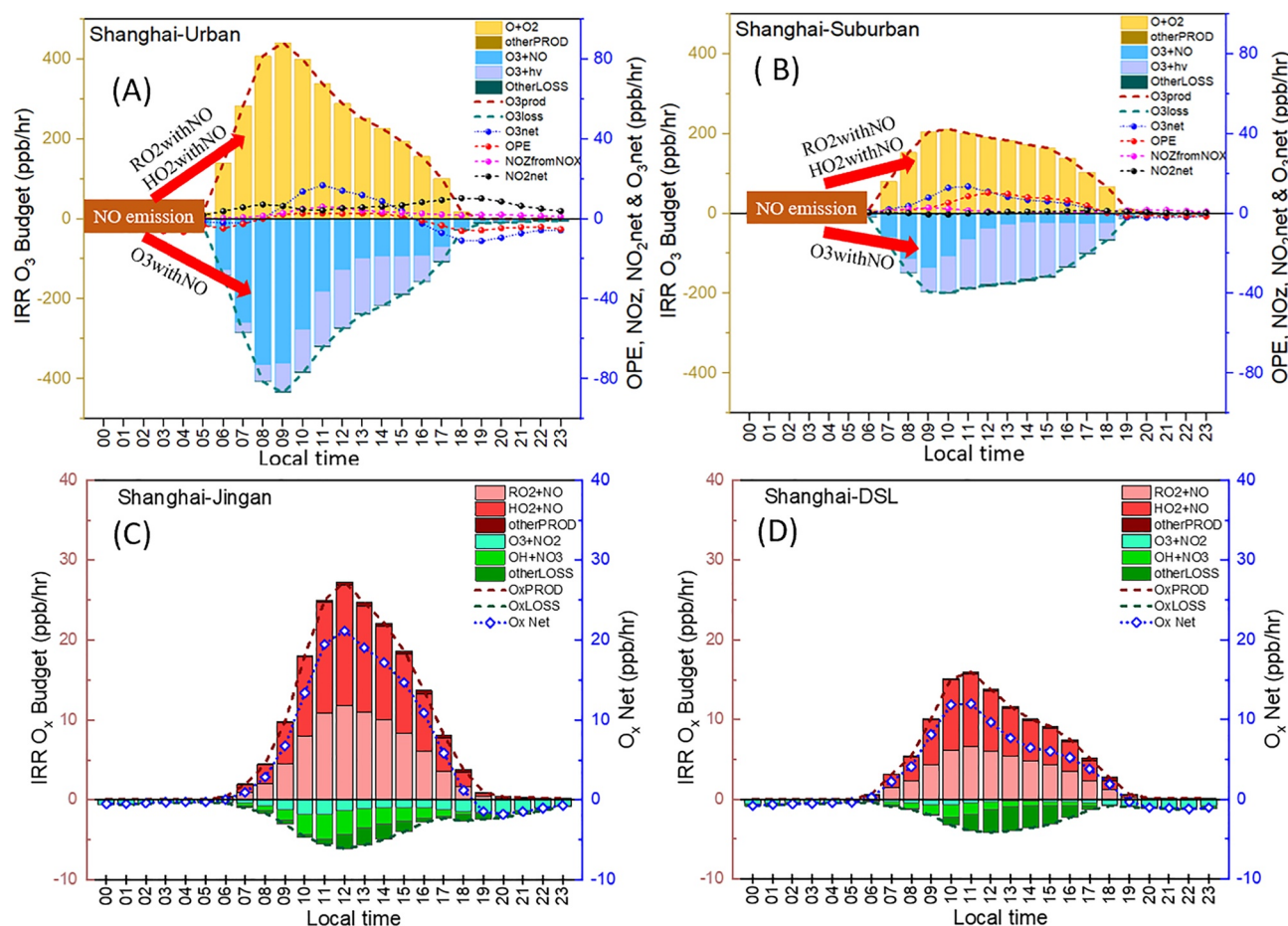
Figure 6. The average diurnal integrated reaction rate budget of (a and b) O_3 and (c and d) O_x within the atmospheric boundary layer at typical urban Jing'an (left) and suburban DSL (right) locations of Shanghai during the O_3 episode period between 24 and 31 July.

pathways involved the reactions of RO_2 + NO and HO_2 + NO, while its main loss pathways were O_3 + NO_2 and OH + NO_3 among others. For O_3, its in situ chemical production pathway is the reaction of O• + O_2, while the chemical loss was mainly via NO-titration (O_3 + NO) and photolysis (O_3 + hv). As an important reactant, O• is mainly from photolysis of NO_2, which is mainly produced from the reaction between RO_2 + NO, HO_2 + NO, and O_3 + NO. The first two reactions dominated the O_x production as shown in Figures 6c and 6d. We also note there are two main loss pathways for the emitted NO, which are (a) the reaction with RO_2 and HO_2 to produce NO_2 without O_3 loss, and (b) the reaction with O_3 to produce NO_2. In general, irrespective of the chemical production/ loss of either O_3 or O_x, the level of photochemical activity at the urban areas was stronger than at the suburban areas. This could be attributed to the intense emissions of pollutants that provide an abundance of reactants in the urban areas (than the suburbs) of Shanghai.

Additionally, during the modeled episode from around 13:00–15:00 LT (at the Jing'an site) and 11:00–15:00 LT (at DSL site), O_3 photolysis was faster than NO-titration (Figures 6a and 6b). It is also evident from Figure 6a that during the early morning hours (6:00–8:00 LT), the production of O_3 from O• + O_2 is less than the O_3 consumed by the reaction O_3 + NO and O_3 photolysis, indicating that the amount of HO_2 and RO_2, which react with NO to produce NO_2, and further produce O•, is relatively small. This is an indication that the chemical formation of O_3 is controlled by VOCs (i.e., VOCs-limited). At noon (and afternoon), the photolysis of O_3 is much enhanced, while the reaction rate of NO + O_3 is significantly lower than the reaction rate of NO + HO_2 and NO + RO_2, indicating that a larger proportion of NO emitted from various sources react with HO_2 and RO_2, which produce NO_2 and further leads to the production of O• via NO_2 photolysis, and a further production of O_3 via the reaction of O• + O_2. Therefore, the pathway from NO with RO_2 and HO_2 is dominant for O_3 production during noon and afternoon, suggesting that there is an abundance of VOCs than NO_x emissions, and with more/less NO_x there

is more/less O_3 produced (i.e., NO_x-limited regime). By comparison, Shanghai suburb site (DSL) has a similar pattern, revealing a strong NO_x-limited conditions from the morning hours (Figure 6b).

From the overall PA results, we noted that gas-phase chemistry played a key role in ground-level O_3 formation during the modeled O_3 episode, and some of the O_3 produced by photochemical process in upper and middle part of the ABL was then transported to the surface via vertical diffusion. Moreover, the dominant contribution of the photochemical processes to surface O_3 did not only last for several days, but was also widespread in areas extending from urban cores into suburban and rural areas of southeastern, central, and northwestern inland regions of YRD (Figure S11 in Supporting Information S1). We also found that during the modeled episode, O_3 formation was aided by various chemical pathways that provided insights and the link between O_3 formation and the responsiveness of O_3 to changes in its precursors (mainly NO_x and VOCs emissions). Therefore, we undertook further quantification of the O_3-NO_x-VOCs sensitivities during the modeled episode to offer vital information needed in the formulation of O_3 mitigation strategy for the region.

3.3. O_3-NO_x-VOCs Sensitivities

3.3.1. Spatial Variability of O_3 Sensitivity

Following the critical role of gas-phase chemistry in the evolution and enhancement of O_3 concentrations during the modeled episode (based on the PA results above), we then examined the response of surface O_3 to the changes in the emissions of its key precursors (NO_x and AVOCs). Figure 7 shows the spatial distribution of daytime O_3-NO_x-VOCs sensitivities over the YRD region between 24 and 31 July 2018. During this episode, O_3 exhibited a wide and clear spatial variability that adequately represents the typical conditions related to daytime evolution of O_3-precursors relationship. In the central and eastern areas of YRD region that exhibited the highest ozone concentrations, the first-order sensitivity coefficients of ozone to AVOCs $\left(S_{O_3\_AVOC}^{(1)}\right)$ and NO_x $\left(S_{O_3\_NO_x}^{(1)}\right)$ were generally higher than 20 µg/m³, and $S_{O_3\_NO_x}^{(1)}$ were largely positive and exceeded $S_{O_3\_AVOC}^{(1)}$ in most areas, except over the urban cores where $S_{O_3\_NO_x}^{(1)}$ were mostly negative in the morning hours (Figure 7). It is understandable that O_3 formation in these urban areas is obviously NO_x-saturated, and hence $S_{O_3\_NO_x}^{(1)}$ is negative while $S_{O_3\_AVOC}^{(1)}$ is positive, which signify a VOCs control regime.

Furthermore, there was a noticeable difference between morning and afternoon O_3 sensitivities during the modeled episode. In some urban areas that present conspicuously blue color as shown in Figure 7c, $S_{O_3\_NO_x}^{(1)}$ is negative in the morning and gradually reduces in proportion and magnitude toward the afternoon hours. As show in Figure 7 and based on the definition of ozone control regimes (see Section 2.3), O_3 tends to be sensitive to VOCs emissions in the morning and begins to switch into a transition regime during the mid-morning hours (and around noon), before expanding into a wider NO_x control regime that even extends to some urban areas in the afternoon. Actually, during morning hours when there is an intense emission of NO_x (mostly due to traffic rush hour), O_3 concentrations are comprehensibly suppressed by depletion caused by the NO-titration effect resulting in the low and mostly negative $S_{O_3\_NO_x}^{(1)}$ (first row Figure 7). Subsequently, from about 10:00 LT as the atmosphere becomes warmer, O_3 concentrations and its sensitivities to NO_x rose sharply (Figure 7c), while the sensitivities to AVOCs showed slight changes. Obviously, as sunny conditions improved more O_3 is produced and its sensitivities intensify because of the increase in photochemical consumption of its precursors. Furthermore, the rapid depletion and declining supply of local NO_x emissions results in an increasingly dominant $S_{O_3\_NO_x}^{(1)}$ in the afternoon as O_3 concentrations peak at about 14:00 LT (fourth row Figure 7c). Interestingly, the second-order sensitivities to NO_x $\left(S_{O_3\_NO_x}^{(2)}\right)$ displayed an opposite sign compared to the $S_{O_3\_NO_x}^{(1)}$ (Figure 7d). It is also notable that in the morning, areas that were conspicuously red shrunk and gradually turned blue (Figure 7d), representing the gradual change of $S_{O_3\_NO_x}^{(2)}$ from positive to negative. This clearly highlights the concave O_3-NO_x response in the morning. In sharp contrast, a convex O_3-NO_x response is prominent over most of the urban areas in the afternoon signifying an accelerated O_3 decrease as NO_x emissions continue to decline. Therefore, to reduce the high concentration of surface O_3 that usually occur in the afternoon over the YRD region, a reduction in NO_x emissions will have a significant effect.

It is important to state that the first- and (non-zero) second-order sensitivities signify, respectively, a linear and nonlinear O_3-precursors relationship, and the matched (unmatched) signs of the second-order sensitivities indicate a convex (concave) O_3 response (Arter & Arunachalam, 2021). In our preliminary investigation, we found
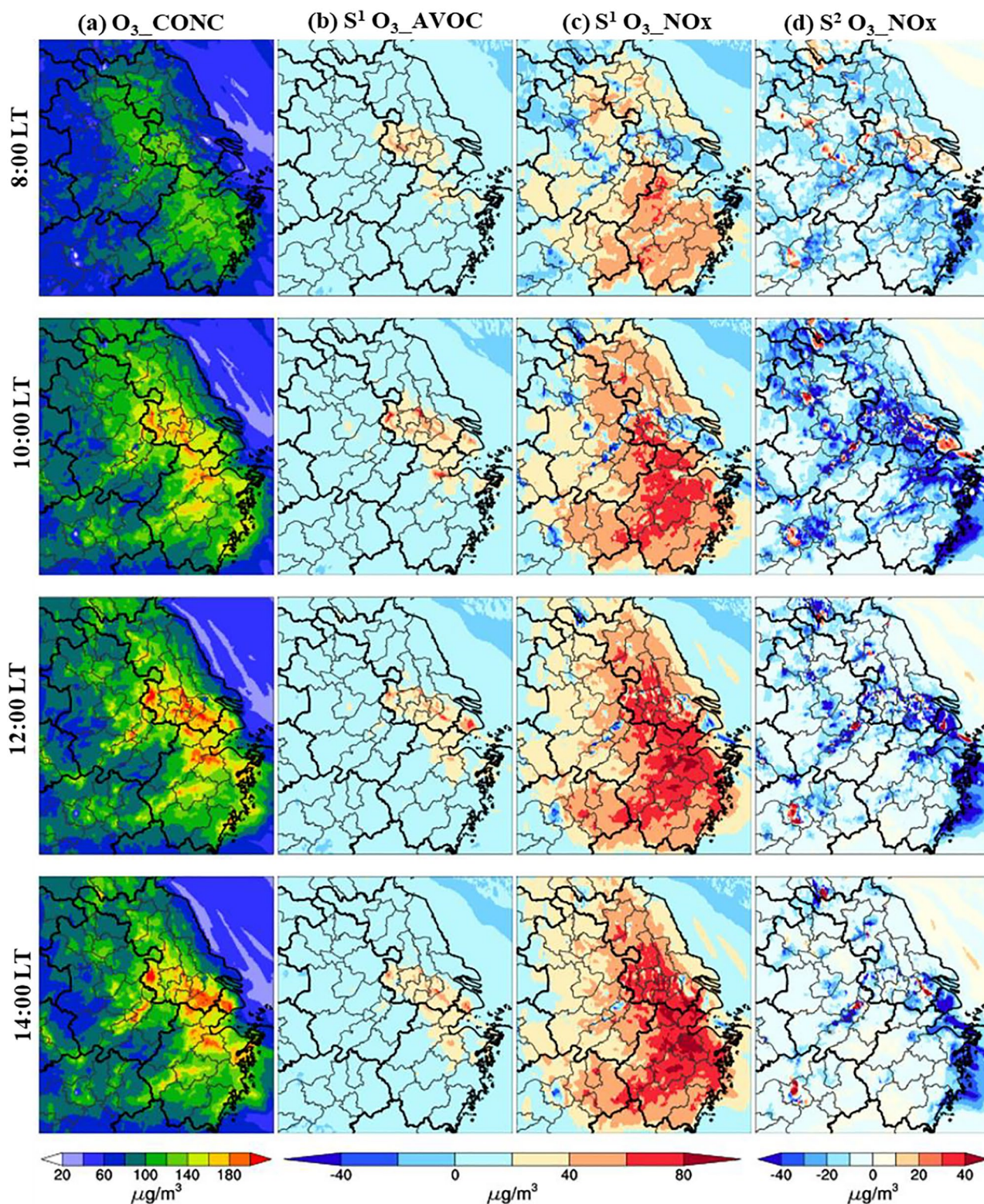
Figure 7. Spatial distribution of daytime (a) O_3 concentration and the respective first-order sensitivity coefficients to (b) AVOCs and (c) NO_x: (d) is 2nd-order sensitivity coefficients to NO_x. The values are average during the episode period between 24 and 31 July 2018 at 9:00 (first-row), 11:00 (second-row), 13:00 (third-row), and 15:00 (fourth-row) local time (LT).

that the second-order sensitivity coefficients to AVOCs $\left(S_{O_3\_AVOC}^{(2)} \right)$ were extremely low (and nearly zero), hence were not considered in the subsequent discussions of this study. This means that O_3 generally exhibits a linear relationship with AVOCs emissions over the YRD region, which can also be evidenced by the minor changes of $S_{O_3\_AVOC}^{(1)}$. On the contrary, non-zero $S_{O_3\_NO_x}^{(2)}$ indicate a nonlinearity of O_3-NO_x relationship, and the larger the magnitudes of $S_{O_3\_NO_x}^{(2)}$ the higher the nonlinearity as shown in Figure 7d. Additionally, the O_3 sensitivity to BVOCs emissions $\left(S_{O_3\_BVOC}^{(1)} \right)$ especially in the southeastern, central, and western inland areas of YRD (not shown), highlights a non-negligible influence of BVOCs on O_3 formation in those areas.

3.3.2. Temporal Variability of Ozone Sensitivity

Figures S12 and S13 in Supporting Information S1 show the temporal variability of $S_{O_3\_NO_x}^{(1)}$, $S_{O_3\_AVOC}^{(1)}$, and $S_{O_3\_BVOC}^{(1)}$ for the period between 17 July to 2 August 2018. Evidently, there is an obvious similarity between the evolution pattern of the sensitivity coefficients and that of O_3 concentrations. Compared to the period between 17 and 23 July, O_3 in all the representative cities exhibited larger magnitudes of $S_{O_3\_NO_x}^{(1)}$, $S_{O_3\_AVOC}^{(1)}$, and $S_{O_3\_BVOC}^{(1)}$ from 24 to 31 July when the severe O_3 episode occurred over the YRD region. Generally, O_3 was significantly sensitive to NO_x emissions than to both the AVOCs and BVOCs with varying magnitudes in the different cities and at different time period. $S_{O_3\_BVOC}^{(1)}$ was significant especially in Nanjing, which is perhaps related to the high temperatures that potentially facilitated heightened generation of more biogenic VOCs emissions. Another notable phenomenon particularly at the suburban MGB monitoring site in Nanjing city is the large magnitudes of negative $S_{O_3\_NO_x}^{(1)}$ compared to the other three cities. This may be largely associated with the larger NO emissions at the MGB site, indicating a stronger titration effect on ozone. Interestingly, although negative $S_{O_3\_NO_x}^{(1)}$ appears frequently in all the key cities, it is generally positive with larger magnitude (than the $S_{O_3\_AVOC}^{(1)}$) during the peak ozone hours in the afternoon, especially in Shanghai and Hangzhou. This is an indication that the control of NO_x emissions in these cities is of greater significance in reducing the high ozone concentration in the afternoon.

Figure 8 further shows the averaged diurnal features of O_3-NO_x-VOCs sensitivities in the four representative cities between 24 and 31 July 2018. It is obvious that the higher the ozone concentration in the afternoon, the greater the sensitivity to precursors, and $S_{O_3\_NO_x}^{(1)}$ was generally positive in all the key cities during the afternoon hours. This hints at the critical roles of NO_x and VOCs in photochemical formation and the diurnal evolution of summertime O_3 pollution over the YRD region. As mentioned above, O_3 in all the key cities tends to be more sensitive to VOCs emissions in the morning hours and shift to be more sensitive to NO_x emissions (or to both NO_x and VOCs) in the afternoon.

In Shanghai for instance, which is the largest city in the YRD region, $S_{O_3\_NO_x}^{(1)}$ and $S_{O_3\_AVOC}^{(1)}$ were highest during the afternoon hours when O_3 was at its peak (Figure 8a). Besides, the large $S_{O_3\_NO_x}^{(1)}$ (positive) and $S_{O_3\_NO_x}^{(2)}$ (negative) in the afternoon suggest that the increasing NO_x emissions would cause an increase in O_3 production with a strong, nonlinear, and convex O_3 response. Similarly, in Hangzhou city $S_{O_3\_AVOC}^{(1)}$ was more pronounced in the morning up to about 11:00 LT as O_3 concentrations rose sharply, before incrementally switching to positive $S_{O_3\_NO_x}^{(1)}$ that dominated the entire afternoon (Figure 8b). Compared with the other cities, O_3 sensitivities in Nanjing city showed significant variability, where considerable negative $S_{O_3\_NO_x}^{(1)}$ and positive $S_{O_3\_NO_x}^{(2)}$ were prevalent in the morning hours (Figure 8c). This indicates that the morning hours O_3 plumes over the selected sites in Nanjing is under a strongly nonlinear concave O_3-NO_x response, which generally elucidates a NO-titration regime. On the contrary, in the afternoon $S_{O_3\_NO_x}^{(1)}$ was positive and $S_{O_3\_NO_x}^{(2)}$ was negative, which further revealed that the increase of NO_x emissions would promote O_3 production with a strongly nonlinear convex O_3 response. In Hefei, which is not only the farthest city downwind among the four representative cities, but it also exhibited the lowest values of O_3-NO_x-VOCs sensitivity during the pollution episode (Figure 8d). This could possibly suggest that besides the local chemical production, O_3 over the selected sites in Hefei is also influenced more by an obvious regional transport from upwind sources. By comparing the suburbs (Figure 8) with the urban sites (Figure S14 in Supporting Information S1), we noted that the latter exhibited lower magnitudes of $S_{O_3\_NO_x}^{(1)}$, which were still significantly higher than the magnitudes of $S_{O_3\_AVOC}^{(1)}$ in the afternoon (especially in Hangzhou).

In general, we found that O_3 was more sensitive to NO_x than VOCs emissions during the afternoon hours, suggesting a good effect of NO_x controls in reducing the high afternoon ozone concentration in all the representative cities. In recent years, the Chinese government has been keen to reduce VOCs emissions with a view of lowering the level of ozone pollution. However, it is worth pointing out that controlling NO_x emissions or reducing the contribution of
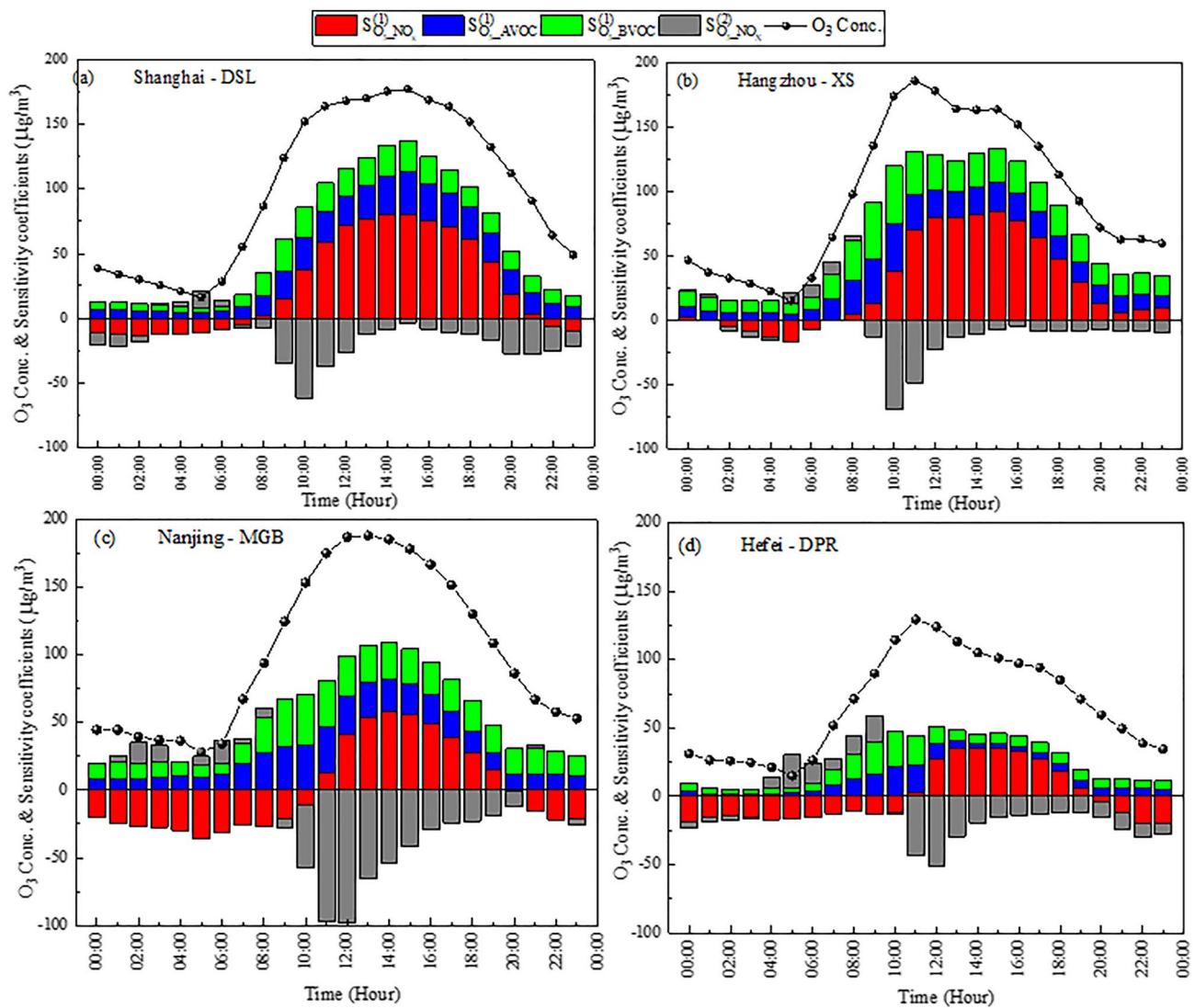
Figure 8. Diurnal profiles of simulated O_3 concentration (black dotted line) and their corresponding first-order sensitivity coefficients to NO_x (red), AVOCs (blue), BVOCs (green) and second-order sensitivity to NO_x (gray) in suburban sites for (a) Shanghai, (b) Hangzhou, (c) Nanjing, and (d) Hefei. The values are averaged over the episode period between 24 and 31 July 2018.

NO_x transport from the upwind areas might be more effective in reducing the afternoon peak ozone concentration in the metropolitan areas (except for cities with particularly large NO emissions) over the YRD region, particularly during similar pollution episodes as considered in this study. Besides, since $S_{O_3\_NO_x}^{(2)}$ were negative in the afternoon while the concentrations of ozone are high, it therefore means that with the continuous reduction of NO_x emission, the reduction rate of O_3 concentrations is accelerated, that is, the effect of ozone mitigation is more significant.

3.4. O_3 Sensitivity Regimes

Average daytime O_3 formation (between 9:00 and 16:00 LT) in the megacities and other urban areas in eastern and central YRD, revealed a clearly defined VOCs-sensitive regime bordered by mixed-sensitivity regimes, while NO_x-sensitive regime dominated most of the other areas (Figure S15 in Supporting Information S1). More specifically, in the morning hours (between 9:00 and 10:00 LT) O_3 formation is visibly under the NO_x-titration regime in most of the eastern coastal areas and central inland regions (Figure 9a), owing to the obvious intense NO_x emissions. In these same areas, NO_x-sensitive regime expanded considerably into areas that were previously under the insensitive regime between 9:00 and 10:00 LT to about 15:00 and 16:00 LT. By around noon, VOCs-sensitive regime had shrunk significantly in Anhui province as it exhibited considerable expansion in the central and
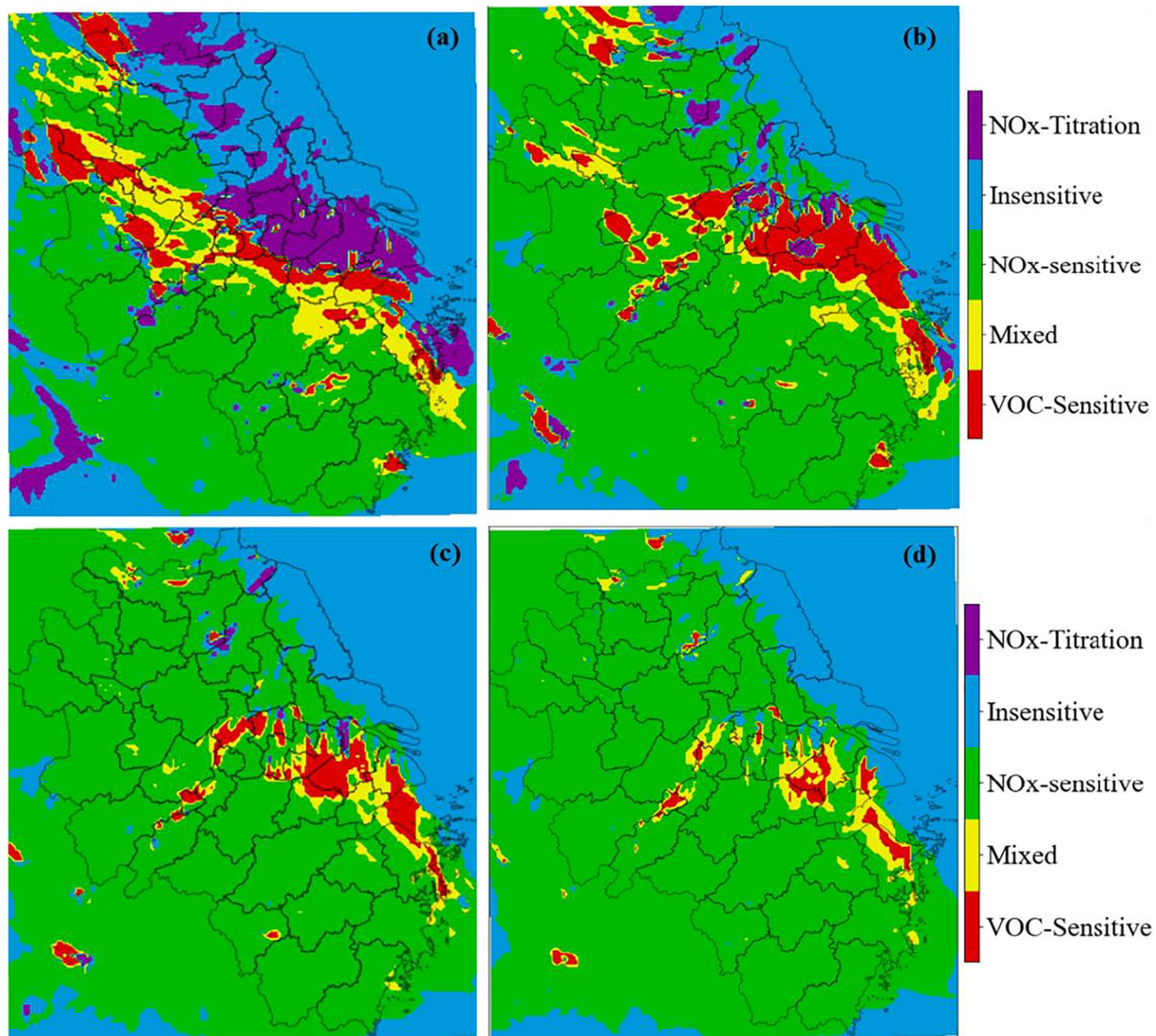
Figure 9. Distribution of O_3 sensitivity regimes averaged between (a) 9:00–10:00 LT, (b) 11:00–12:00 LT, (c) 13:00–14:00 LT, (d) 15:00–16:00 LT during a severe O_3 episode on 24−31 July 2018 over the Yangtze River Delta region. The different colors correspond to the different sensitivity regimes: VOCs-sensitive (red), NO_x-sensitive (green), mixed sensitivity (yellow), NO_x-titration (purple) and insensitive (blue) regimes.

eastern areas of YRD (Figure 9b). Meanwhile, NO_x-titration regime significantly reduced with time, and almost disappeared in the afternoon (Figures 9c and 9d). Overall, the afternoon O_3 formation in almost the entire YRD domain was largely under the NO_x-sensitive regime with very few locations exhibiting VOCs-sensitive and mixed sensitivity regimes.

Further classification of the daytime hourly $S_{O_3\_NO_x}^{(1)}$ and $S_{O_3\_AVOC}^{(1)}$ during the episode period is shown for the typical suburban (Figure 10) and urban (Figure S16 in Supporting Information S1) sites of the four representative cities. O_3 formation in the morning hours before 9:00 LT was mostly and obviously either in the NO_x titration regime or the VOCs sensitive regime, even though some O_3 plumes were generally under an insensitive regime in the early morning and late afternoon hours. However, at both the suburban and urban sites, the NO_x sensitive regime was increasingly dominant from around noon, except for the urban JA site in Shanghai where the mixed sensitive regime dominated with strong sensitivities to both NO_x and VOCs. Our results are in general agreement with a previous study by N. Wang et al. (2019) that found gradual shifting of summertime O_3 formation from VOCs-sensitive toward a more mixed-sensitivity regime in YRD as a result of recent NO_x reductions. Nevertheless, our results provide a wider and more comprehensive O_3-NO_x-VOCs relationship that can be quite
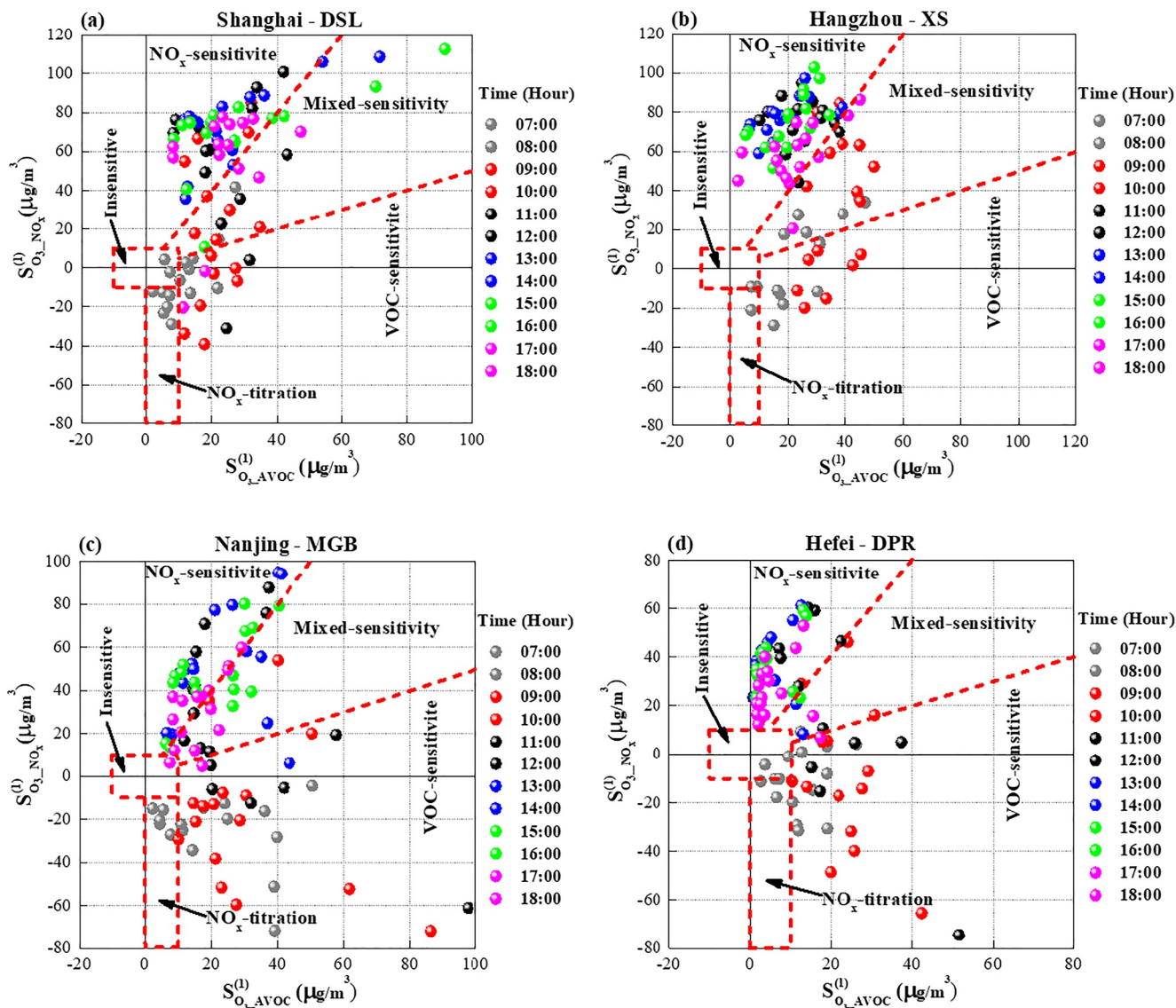
Figure 10. Scatter plots for hourly O_3 sensitivity coefficients to AVOCs (*x*-axis) and NO_x (*y*-axis) during from 7:00 to 18:00 LT at suburban sites in (a) Shanghai (b) Hangzhou (c) Nanjing and (d) Hefei during severe O_3 episode between 24 and 31 July. The various categories of O_3 sensitivity regimes are classified using red dotted lines (Insensitive, NO_x-sensitive, mix-sensitivity, VOC-sensitive, and NO_x-titration regimes) accordingly.

important for governments to take more precise and effective measures to mitigate O_3 pollution in the YRD region.

3.5. Comparison of HDDM With the Brute Force Method

In addition to evaluating the performance of the base CMAQ model (see Section 3.1), we also assessed the truthfulness of the sensitivities computed by the HDDM tool. It is worth noting that evaluating the accuracy of sensitivity analysis results is inherently challenging, especially because the responsiveness of ambient concentrations to changes in precursor emissions cannot be directly observed in the atmosphere due to meteorological conditions (which cannot be held constant) (Cohan & Napelenok, 2011). Therefore, the precision and the integral purpose of the AQM used for the simulation is critical. Essentially, the accuracy of the technique used for sensitivity analysis is assessed based on its degree of effectiveness in capturing the relationships within the AQM. This implies that the performance of the AQM instrumented with the HDDM-3D tool is fundamental in making a determination of the computed sensitivities. Therefore, having found an acceptable model performance in
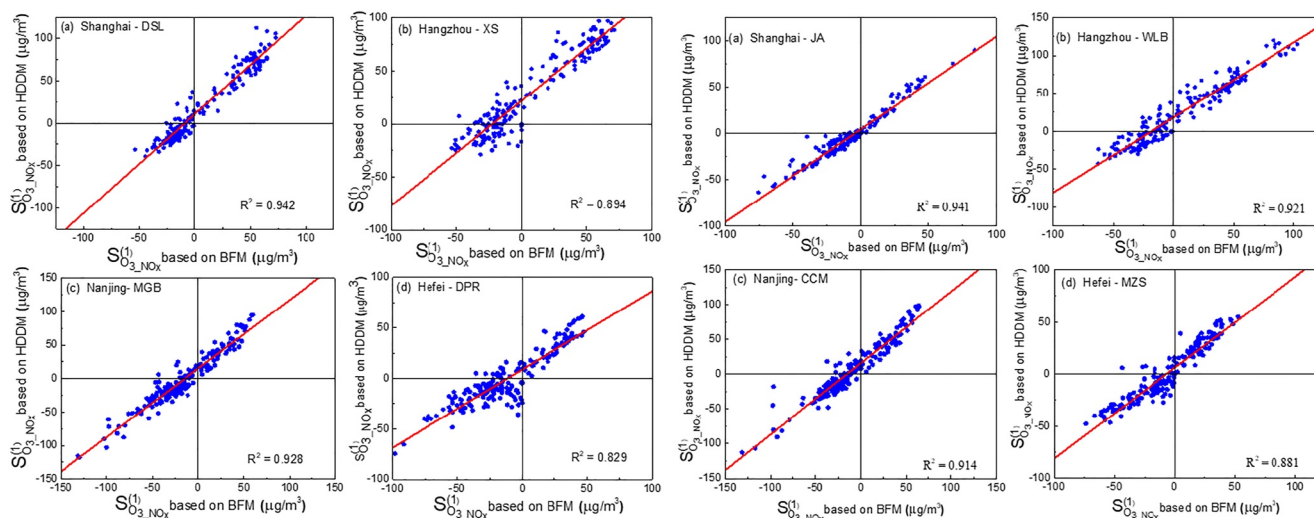
Figure 11. Scatter plots showing the comparison of BFM (*x*-axis) and HDDM (*y*-axis) for ozone sensitivity to NO_x emissions averaged during the O_3 episode between 24 and 31 July at the suburban and urban sites of the four representative cities in Yangtze River Delta. The high level of correlation reveals that their sensitivities are in close agreement.

replicating the observed pollutant concentrations (see Text S1 in Supporting Information S1), we then compared the first-order HDDM sensitivity coefficients with those obtained using the BFM, which was applied in related studies (Dunker et al., 2002; Hakami et al., 2004; W. Zhang et al., 2012).

In our validation, the consistency, and an estimate of the accuracy of HDDM sensitivities is tested by considering BFM runs with a 10% perturbation in NO_x emissions to calculate $S^{(1)}_{O_3\_NO_x}$ based on the finite differencing method:

$$S^{(1)}_{O_3\_NO_x} \approx \frac{C^{110\%NO_x} - C^{90\%NO_x}}{2\Delta\varepsilon_{NOx}} \tag{6}$$

where C is the concentration of O_3 ($\mu g/m^3$) for the BFM runs of $\pm10\%$ perturbations in NO_x emissions. As shown in Figure 11, the performance of HDDM is highly consistent with the BFM both in terms of magnitudes and the spatial pattern of $S^{(1)}_{O_3\_NO_x}$. For that reason, the HDDM method has sufficient reliability to analyze the O_3-NO_x-VOCs sensitivity and the corresponding identification of chemical regimes over the YRD region.

4. Conclusion

Based on the WRF model and the CMAQ model embedded with HDDM-3D and PA tools, this study explored, quantified, and comprehended the spatiotemporal characteristics of integrated process rate and integrated reaction rate, as well as the domain-wide O_3-NO_x-VOCs relationship during a typical O_3 pollution episode between 24 and 31 July 2018. Ultimately, we propose efficient pathways to mitigate ozone pollution in the YRD region having arrived at several conclusions.

During the modeled episode, gas-phase chemistry contributed dominantly to the ground-level O_3, a significant proportion of which was chemically produced in the upper and middle part of the ABL and was then transported to the surface via vertical diffusion. Furthermore, we found that in situ chemical reaction contributed more to the increase of ozone in the upper zone within the boundary layer than at the ground-level. On the other hand, the O_3 chemical capacity in the surface was much higher than the upper zone considering the significant contribution of chemical reaction to O_x ($O_3 + NO_2$). Irrespective of the production/loss of either O_3 or O_x, the photochemical activity level is stronger in urban areas than the suburbs (especially in Shanghai). This is mainly due to the strong emissions of pollutants that provide large quantities of reactants in the urban areas. The IRR analysis further revealed the main chemical pathways that contributed to O_3 formation during the episode, thus providing important insights into linking O_3 formation and its sensitivities to precursors (NO_x and VOCs emissions), and which were consistent with the HDDM results.

There is a wide variability in the sensitivities of O_3 to domain-wide NO_x and VOCs emissions during the simulated O_3 episode. The peak hourly O_3 concentration between 24 and 31 July was mainly sensitive to both NO_x and AVOC emissions especially in the urbanized areas in eastern and central YRD. Although the first-order sensitivity of O_3 to AVOCs over the YRD region was mainly positive, with lower magnitudes and minimal overall changes, and thus the second-order sensitivity coefficients were extremely low and negligible.

On the other hand, the first-order sensitivity of O_3 to NO_x exhibited wide variations most of which were positive, and were much larger than those to AVOCs in the afternoon at the time when O_3 levels peaked even within the urban areas of Shanghai, Hangzhou, Nanjing, and Hefei. It is only over a few locations (particularly in the urban cores) that the first-order sensitivity of O_3 to NO_x was negative mostly in the morning. Besides, the second-order sensitivity coefficients to NO_x gradually changed from morning (positive) to afternoon (negative), showing a concave and convex response, respectively, over these urban areas. This means that as NO_x continues to decrease, the rate of ground-level O_3 decrease accelerates in the afternoon. Therefore, reducing the peak O_3 concentrations in the afternoon via NO_x emission controls will be more effective even in the metropolis. Admittedly, the effects of NO_x emission control were all pronounced in all the non-urban areas due to the conspicuously positive O_3-NO_x sensitivity. In addition, the sensitivity of O_3 to BVOCs emissions in the southeastern, central, and western inland areas of YRD signifies a non-negligible influence of BVOCs on O_3 formation in those areas.

To sum up, the Chinese government has made great efforts to control VOCs emissions in recent years in order to mitigate ozone pollution. However, the effect of these efforts over the years has not been obvious. To date, mitigating ozone pollution remains a challenge not only over the YRD region, but also in many other cities in China. The results of this study emphasize the importance of local and upwind NO_x emissions control to mitigate the afternoon peak O_3 concentrations during similar O_3 episode in the most of YRD region, even in urban areas.

Conflict of Interest

The authors declare no conflicts of interest relevant to this study.

Data Availability Statement

All data used in this paper has been deposited in an open research depository, accessible at https://doi.org/10.17632/tc9jt5c4mh.2 (Y. Wang et al., 2022) or https://pan.baidu.com/s/1l3rycjfJkmJ_Uz_YuoLRRw?pwd=3462 (last access: June 2022), the file name is: "The importance of NOx control for peak ozone Using CMAQ-HDDM over YRD.xlsx." Weather observations data sets ds351.0 and ds461.0, as well as ds083.2 were used for data assimilation and input for the WRF, and are available in the research data archive maintained by the National Center for Atmospheric Research via https://doi.org/10.5065/39C5-Z211 (The National Centers for Environmental Prediction et al., 2018b), https://doi.org/10.5065/4F4P-E398 (The National Centers for Environmental Prediction et al., 2018a), and https://doi.org/10.5065/D6M043C6 (The National Centers for Environmental Prediction et al., 2018c), respectively. The Multi-resolution Emission Inventory for China is available at: http://www.meic-model.org. Version 5.3.2 of the community multiscale air quality (CMAQ) model used for higher-order decouple direct method (HDDM) and process analysis (PA) is preserved at https://www.cmascenter.org (US Environmental Protection Agency, 2020) and developed openly by US Environmental Protection Agency, accessible at https://www.epa.gov/cmaq.

References

Arter, C. A., & Arunachalam, S. (2021). Assessing the importance of nonlinearity for aircraft emissions' impact on O_3 and $PM_{2.5}$. *Science of the Total Environment*, *777*, 146121. https://doi.org/10.1016/j.scitotenv.2021.146121

Brancher, M. (2021). Increased ozone pollution alongside reduced nitrogen dioxide concentrations during Vienna's first COVID-19 lockdown: Significance for air quality management. *Environmental Pollution*, *284*, 117153. https://doi.org/10.1016/j.envpol.2021.117153

Chen, K., Zhou, L., Chen, X., Bi, J., & Kinney, P. L. (2017). Acute effect of ozone exposure on daily mortality in seven cities of Jiangsu Province, China: No clear evidence for threshold. *Environmental Research*, *155*, 235–241. https://doi.org/10.1016/j.envres.2017.02.009

Cohan, D. S., & Napelenok, S. L. (2011). Air quality response modeling for decision support. *Atmosphere*, *2*(3), 407–425. https://doi.org/10.3390/atmos2030407

Ding, A. J., Fu, C. B., Yang, X. Q., Sun, J. N., Zheng, L. F., Xie, Y. N., et al. (2013). Ozone and fine particle in the western Yangtze River Delta: An overview of 1 yr data at the SORPES station. *Atmospheric Chemistry and Physics*, *13*(11), 5813–5830. https://doi.org/10.5194/acp-13-5813-2013

Dunker, A. M., Yarwood, G., Ortmann, J. P., & Wilson, G. M. (2002). The decoupled direct method for sensitivity analysis in a three-dimensional air quality model implementation, accuracy, and efficiency. *Environmental Science & Technology*, *36*(13), 2965–2976. https://doi.org/10.1021/es0112691

Feng, R., Wang, Q., Huang, C.-C., Liang, J., Luo, K., Fan, J.-R., & Zheng, H. J. (2019). Ethylene, xylene, toluene and hexane are major contributors of atmospheric ozone in Hangzhou, China, prior to the 2022 Asian Games. *Environmental Chemistry Letters*, *17*(2), 1151–1160. https://doi.org/10.1007/s10311-018-00846-w

Hakami, A., Odman, M. T., & Russell, A. G. (2003). High-order, direct sensitivity analysis of multidimensional air quality models. *Environmental Science & Technology*, *37*(11), 2442–2452. https://doi.org/10.1021/es020677h

Hakami, A., Odman, M. T., & Russell, A. G. (2004). Nonlinearity in atmospheric response: A direct sensitivity analysis approach. *Journal of Geophysical Research: Atmospheres*, *109*(D15), D15303. https://doi.org/10.1029/2003jd004502

Han, L., Chen, L., Li, K., Bao, Z., Zhao, Y., Zhang, X., et al. (2019). Source apportionment of volatile organic compounds (VOCs) during ozone polluted days in Hangzhou, China. *Atmosphere*, *10*(12), 780. https://doi.org/10.3390/atmos10120780

Hu, J., Li, Y. C., Zhao, T. L., Liu, J., Hu, X. M., Liu, D. Y., et al. (2018). An important mechanism of regional O_3 transport for summer smog over the Yangtze River Delta in eastern China. *Atmospheric Chemistry and Physics*, *18*(22), 16239–16251. https://doi.org/10.5194/acp-18-16239-2018

Huang, Z., Hu, Y., Zheng, J., Yuan, Z., Russell, A. G., Ou, J., & Zhong, Z. (2017). A new combined stepwise-based high-order decoupled direct and reduced-form method to improve uncertainty analysis in $PM_{2.5}$ simulations. *Environmental Science & Technology*, *51*(7), 3852–3859. https://doi.org/10.1021/acs.est.6b05479

Huang, Z., Zheng, J., Ou, J., Zhong, Z., Wu, Y., & Shao, M. (2019). A feasible methodological framework for uncertainty analysis and diagnosis of atmospheric chemical transport models. *Environmental Science & Technology*, *53*(6), 3110–3118. https://doi.org/10.1021/acs.est.8b06326

Jiang, Z., Li, J., Lu, X., Gong, C., Zhang, L., & Liao, H. (2021). Impact of western Pacific subtropical high on ozone pollution over eastern China. *Atmospheric Chemistry and Physics*, *21*(4), 2601–2613. https://doi.org/10.5194/acp-21-2601-2021

Jin, L., Tonse, S., Cohan, D. S., Mao, X., Harley, R. A., & Brown, N. J. (2008). Sensitivity analysis of ozone formation and transport for a central California air pollution episode. *Environmental Science & Technology*, *42*(10), 3683–3689. https://doi.org/10.1021/es072069d

Jin, X. M., & Holloway, T. (2015). Spatial and temporal variability of ozone sensitivity over China observed from the Ozone Monitoring Instrument. *Journal of Geophysical Research: Atmospheres*, *120*(14), 7229–7246. https://doi.org/10.1002/2015jd023250

Li, D. R., Wang, S. S., Xue, R. B., Zhu, J., Zhang, S. B., Sun, Z. B., & Zhou, B. (2021). OMI-observed HCHO in Shanghai, China, during 2010–2019 and ozone sensitivity inferred by an improved $HCHO/NO_2$ ratio. *Atmospheric Chemistry and Physics*, *21*(20), 15447–15460. https://doi.org/10.5194/acp-21-15447-2021

Li, L., Chen, C., Huang, C., Huang, H., Zhang, G., Wang, Y., et al. (2011). Ozone sensitivity analysis with the MM5-CMAQ modeling system for Shanghai. *Journal of Environmental Sciences*, *23*(7), 1150–1157. https://doi.org/10.1016/s1001-0742(10)60527-x

Li, L., Li, Q., Huang, L., Wang, Q., Zhu, A., Xu, J., et al. (2020). Air quality changes during the COVID-19 lockdown over the Yangtze River Delta Region: An insight into the impact of human activity pattern changes on air pollution variation. *Science of the Total Environment*, *732*, 139282. https://doi.org/10.1016/j.scitotenv.2020.139282

Lin, C., Leung, K. K. M., Yu, A. L. C., Tsang, R. C. W., Tsui, W. B. C., Fung, J. C. H., et al. (2021). Effects of synoptic patterns on the vertical structure of ozone in Hong Kong using lidar measurement. *Atmospheric Environment*, *257*, 118490. https://doi.org/10.1016/j.atmosenv.2021.118490

Liu, H., Liu, J., Liu, Y., Yi, K., Yang, H., Xiang, S., et al. (2021). Spatiotemporal variability and driving factors of ground-level summertime ozone pollution over eastern China. *Atmospheric Environment*, *265*, 118686. https://doi.org/10.1016/j.atmosenv.2021.118686

Liu, Y., Song, M., Liu, X., Zhang, Y., Hui, L., Kong, L., et al. (2020). Characterization and sources of volatile organic compounds (VOCs) and their related changes during ozone pollution days in 2016 in Beijing, China. *Environmental Pollution*, *257*, 113599. https://doi.org/10.1016/j.envpol.2019.113599

Liu, Y., & Wang, T. (2020). Worsening urban ozone pollution in China from 2013 to 2017 – Part 2: The effects of emission changes and implications for multi-pollutant control. *Atmospheric Chemistry and Physics*, *20*(11), 6323–6337. https://doi.org/10.5194/acp-20-6323-2020

Luecken, D. J., Napelenok, S. L., Strum, M., Scheffe, R., & Phillips, S. (2018). Sensitivity of ambient atmospheric formaldehyde and ozone to precursor species and source types across the United States. *Environmental Science & Technology*, *52*(8), 4668–4675. https://doi.org/10.1021/acs.est.7b05509

Lyu, X. P., Chen, N., Guo, H., Zhang, W. H., Wang, N., Wang, Y., & Liu, M. (2016). Ambient volatile organic compounds and their effect on ozone production in Wuhan, central China. *Science of the Total Environment*, *541*, 200–209. https://doi.org/10.1016/j.scitotenv.2015.09.093

Mao, J., Ren, X., Chen, S., Brune, W. H., Chen, Z., Martinez, M., et al. (2010). Atmospheric oxidation capacity in the summer of Houston 2006: Comparison with summer measurements in other metropolitan studies. *Atmospheric Environment*, *44*(33), 4107–4115. https://doi.org/10.1016/j.atmosenv.2009.01.013

Pan, X., Kanaya, Y., Tanimoto, H., Inomata, S., Wang, Z., Kudo, S., & Uno, I. (2015). Examining the major contributors of ozone pollution in a rural area of the Yangtze River Delta region during harvest season. *Atmospheric Chemistry and Physics*, *15*(11), 6101–6111. https://doi.org/10.5194/acp-15-6101-2015

Pleijel, H., Broberg, M. C., Uddling, J., & Mills, G. (2018). Current surface ozone concentrations significantly decrease wheat growth, yield and quality. *Science of the Total Environment*, *613–614*, 687–692. https://doi.org/10.1016/j.scitotenv.2017.09.111

Ren, X., van Duin, D., Cazorla, M., Chen, S., Mao, J., Zhang, L., et al. (2013). Atmospheric oxidation chemistry and ozone production: Results from SHARP 2009 in Houston, Texas. *Journal of Geophysical Research: Atmospheres*, *118*(11), 5770–5780. https://doi.org/10.1002/jgrd.50342

Shen, H., Sun, Z., Chen, Y., Russell, A. G., Hu, Y., Odman, M. T., et al. (2021). Novel method for ozone isopleth construction and diagnosis for the ozone control strategy of Chinese cities. *Environmental Science & Technology*, *55*(23), 15625–15636. https://doi.org/10.1021/acs.est.1c01567

Shu, L., Wang, T., Han, H., Xie, M., Chen, P., Li, M., & Wu, H. (2020). Summertime ozone pollution in the Yangtze River Delta of eastern China during 2013–2017: Synoptic impacts and source apportionment. *Environmental Pollution*, *257*, 113631. https://doi.org/10.1016/j.envpol.2019.113631

Shu, L., Xie, M., Wang, T., Gao, D., Chen, P., Han, Y., et al. (2016). Integrated studies of a regional ozone pollution synthetically affected by subtropical high and typhoon system in the Yangtze River Delta region, China. *Atmospheric Chemistry and Physics*, *16*(24), 15801–15819. https://doi.org/10.5194/acp-16-15801-2016

Sillman, S., & West, J. J. (2009). Reactive nitrogen in Mexico city and its relation to ozone-precursor sensitivity: Results from photochemical models. *Atmospheric Chemistry and Physics*, *9*(11), 3477–3489. https://doi.org/10.5194/acp-9-3477-2009

Tan, Z., Lu, K., Jiang, M., Su, R., Wang, H., Lou, S., et al. (2019). Daytime atmospheric oxidation capacity in four Chinese megacities during the photochemically polluted season: A case study based on box model simulation. *Atmospheric Chemistry and Physics*, *19*(6), 3493–3513. https://doi.org/10.5194/acp-19-3493-2019

The National Centers for Environmental Prediction. (2018a). NCEP ADP global surface observational weather data. ds461.0 [Dataset]. Research Data Archive at the National Center for Atmospheric Research, Computational and Information Systems Laboratory. https://doi.org/10.5065/4F4P-E398

The National Centers for Environmental Prediction. (2018b). NCEP ADP global upper air observational weather data. ds351.0 [Dataset]. Research Data Archive at the National Center for Atmospheric Research, Computational and Information Systems Laboratory. https://doi.org/10.5065/39C5-Z211/

The National Centers for Environmental Prediction. (2018c). NCEP FNL operational model global tropospheric analyses. ds083.2 [Dataset]. Research Data Archive at the National Center for Atmospheric Research, Computational and Information Systems Laboratory. https://doi.org/10.5065/D6M043C6

US Environmental Protection Agency. (2020). CMAQ 5.3.2 [Software]. CMAS. Retrieved from https://www.cmascenter.org/

Wang, M., Chen, W., Zhang, L., Qin, W., Zhang, Y., Zhang, X., & Xie, X. (2020). Ozone pollution characteristics and sensitivity analysis using an observation-based model in Nanjing, Yangtze River Delta Region of China. *Journal of Environmental Sciences*, *93*, 13–22. https://doi.org/10.1016/j.jes.2020.02.027

Wang, N., Lyu, X., Deng, X., Huang, X., Jiang, F., & Ding, A. (2019). Aggravating O₃ pollution due to NOₓ emission control in eastern China. *Science of the Total Environment*, *677*, 732–744. https://doi.org/10.1016/j.scitotenv.2019.04.388

Wang, T., Xue, L. K., Brimblecombe, P., Lam, Y. F., Li, L., & Zhang, L. (2017). Ozone pollution in China: A review of concentrations, meteorological influences, chemical precursors, and effects. *Science of the Total Environment*, *575*, 1582–1596. https://doi.org/10.1016/j.scitotenv.2016.10.081

Wang, X., Zhang, Y., Hu, Y., Zhou, W., Zeng, L., Hu, M., et al. (2011). Decoupled direct sensitivity analysis of regional ozone pollution over the Pearl River Delta during the PRIDE-PRD2004 campaign. *Atmospheric Environment*, *45*(28), 4941–4949. https://doi.org/10.1016/j.atmosenv.2011.06.006

Wang, Y., Yaluk, E., Chen, H., Jiang, S., Huang, L., Zhu, A., et al. (2022). The importance of NOₓ control for peak ozone mitigation based on a sensitivity study using CMAQ-HDDM-3D model during a typical episode over the Yangtze River Delta region, China [Dataset]. Mendeley Data. https://doi.org/10.17632/tc9jt5c4mh.2

Wang, Y. L., Wild, O., Ashworth, K., Chen, X. S., Wu, Q. Z., Qi, Y., & Wang, Z. (2022). Reductions in crop yields across China from elevated ozone. *Environmental Pollution*, *292*, 118218. https://doi.org/10.1016/j.envpol.2021.118218

Watson, R., Rodhe, H., & Oeschger, H. (1990). Greenhouse gases and aerosols. *Scientific Assessment of Climate Change: Report* (Vol. *1*).

Wei, W., Li, Y., Ren, Y., Cheng, S., & Han, L. (2019). Sensitivity of summer ozone to precursor emission change over Beijing during 2010–2015: A WRF-chem modeling study. *Atmospheric Environment*, *218*, 116984. https://doi.org/10.1016/j.atmosenv.2019.116984

Xu, J., Huang, X., Wang, N., Li, Y., & Ding, A. (2021). Understanding ozone pollution in the Yangtze River Delta of eastern China from the perspective of diurnal cycles. *Science of the Total Environment*, *752*, 141928. https://doi.org/10.1016/j.scitotenv.2020.141928

Xue, L. K., Wang, T., Gao, J., Ding, A. J., Zhou, X. H., Blake, D. R., et al. (2014). Ground-level ozone in four Chinese cities: Precursors, regional transport and heterogeneous processes. *Atmospheric Chemistry and Physics*, *14*(23), 13175–13188. https://doi.org/10.5194/acp-14-13175-2014

Yarwood, G., Emery, C., Jung, J., Nopmongcol, U., & Sakulyanontvittaya, T. (2013). A method to represent ozone response to large changes in precursor emissions using high-order sensitivity analysis in photochemical models. *Geoscientific Model Development*, *6*(5), 1601–1608. https://doi.org/10.5194/gmd-6-1601-2013

Yu, Y., Wang, Z., He, T., Meng, X., Xie, S., & Yu, H. (2019). Driving factors of the significant increase in surface ozone in the Yangtze River Delta, China, during 2013–2017. *Atmospheric Pollution Research*, *10*(4), 1357–1364. https://doi.org/10.1016/j.apr.2019.03.010

Zhan, C., Xie, M., Huang, C., Liu, J., Wang, T., Xu, M., et al. (2020). Ozone affected by a succession of four landfall typhoons in the Yangtze River Delta, China: Major processes and health impacts. *Atmospheric Chemistry and Physics*, *20*(22), 13781–13799. https://doi.org/10.5194/acp-20-13781-2020

Zhang, J., Li, D., Bian, J., Xuan, Y., Chen, H., Bai, Z., et al. (2021). Long-term ozone variability in the vertical structure and integrated column over the North China plain: Results based on ozonesonde and Dobson measurements during 2001-2019. *Environmental Research Letters*, *16*(7), 074053. https://doi.org/10.1088/1748-9326/ac109f

Zhang, W., Capps, S. L., Hu, Y., Nenes, A., Napelenok, S. L., & Russell, A. G. (2012). Development of the high-order decoupled direct method in three dimensions for particulate matter: Enabling advanced sensitivity analysis in air quality models. *Geoscientific Model Development*, *5*(2), 355–368. https://doi.org/10.5194/gmd-5-355-2012

Zhang, W., Trail, M. A., Hu, Y., Nenes, A., & Russell, A. G. (2015). Use of high-order sensitivity analysis and reduced-form modeling to quantify uncertainty in particulate matter simulations in the presence of uncertain emissions rates: A case study in Houston. *Atmospheric Environment*, *122*, 103–113. https://doi.org/10.1016/j.atmosenv.2015.08.091

Zhao, D., Xin, J., Wang, W., Jia, D., Wang, Z., Xiao, H., et al. (2022). Effects of the sea-land breeze on coastal ozone pollution in the Yangtze River Delta, China. *Science of the Total Environment*, *807*, 150306. https://doi.org/10.1016/j.scitotenv.2021.150306

References From the Supporting Information

Emery, C., Liu, Z., Russell, A. G., Odman, M. T., Yarwood, G., & Kumar, N. (2017). Recommendations on statistics and benchmarks to assess photochemical model performance. *Journal of the Air & Waste Management Association*, *67*(5), 582–598. https://doi.org/10.1080/10962247.2016.1265027

Huang, L., Wang, Q., Wang, Y., Emery, C., Zhu, A., Zhu, Y., et al. (2021). Simulation of secondary organic aerosol over the Yangtze River Delta region: The impacts from the emissions of intermediate volatility organic compounds and the SOA modeling framework. *Atmospheric Environment*, *246*, 118079. https://doi.org/10.1016/j.atmosenv.2020.118079

Liu, T., Wang, X. Y., Hu, J. L., Wang, Q., An, J. Y., Gong, K. J., et al. (2020). Driving forces of changes in air quality during the COVID-19 lockdown period in the Yangtze River Delta region, China. *Environmental Science and Technology Letters*, *7*(11), 779–786. https://doi.org/10.1021/acs.estlett.0c00511

Shi, L., Zhu, A., Huang, L., Yaluk, E., Gu, Y., Wang, Y., et al. (2021). Impact of the planetary boundary layer on air quality simulations over the Yangtze River Delta region, China. *Atmospheric Environment*, *263*, 118685. https://doi.org/10.1016/j.atmosenv.2021.118685

Wang, H. L., Huang, C., Tao, W., Gao, Y. Q., Wang, S. W., Jing, S. A., et al. (2022). Seasonality and reduced nitric oxide titration dominated ozone increase during COVID-19 lockdown in eastern China. *Npj Climate and Atmospheric Science*, *5*(1), 24. https://doi.org/10.1038/s41612-022-00249-3

Wang, X. Y., Li, L., Gong, K. J., Mao, J. J., Hu, J. L., Li, J. Y., et al. (2021). Modelling air quality during the EXPLORE-YRD campaign-Part I. Model performance evaluation and impacts of meteorological inputs and grid resolutions. *Atmospheric Environment*, *246*, 118131. https://doi.org/10.1016/j.atmosenv.2020.118131